

Simulations of Discrete Random Geometries:
Simplicial Quantum Gravity
and
Quantum String Theory

Dissertation zur Erlangung des Doktorgrades
vorgelegt von
Joachim Tabaczek

November 4, 2018

I investigate two discrete models of random geometries, namely simplicial quantum gravity and quantum string theory.

In four-dimensional simplicial quantum gravity, I show that the addition of matter gauge fields to the model is capable of changing its phase structure by replacing the branched polymers of the pure gravity model with a new phase that has a negative string susceptibility exponent and a fractal dimension of four. Some of the results are derived from a strong coupling expansion of the model, a technique which is used here for the first time in this context.

In quantum string theory, I study a discrete version of the *IIB* superstring. I show that the divergences encountered in the discretization of the bosonic string are eliminated in the supersymmetric case. I give theoretical arguments for the appearance of one-dimensional structures in the region of large system extents that manifest as a power-law tail in the link length distribution; this is confirmed by numerical simulations of the model. I also examine a lower-dimensional version of the *IKKT* matrix model, in which a similar effect can be observed.

Contents

1	Introduction	1
2	Dynamical triangulations	3
2.1	Simplicial manifolds	3
2.1.1	Definition of a simplicial manifold	3
2.1.2	The discrete metric	5
2.2	Numerical simulations	7
2.2.1	Monte Carlo algorithms	7
2.2.2	Transformations	10
3	The strong coupling expansion in simplicial quantum gravity	13
3.1	Simplicial quantum gravity	13
3.1.1	Discretization of pure gravity	15
3.1.2	The structure of space-time	17
3.1.3	The two-dimensional case	19
3.1.4	The four-dimensional case	21
3.2	Modifications of the model	22
3.2.1	Matter fields	22
3.2.2	Measure terms	24
3.3	The strong coupling expansion	24
3.3.1	Calculation of the series terms	24
3.3.2	The ratio method	27
3.3.3	Results	28
3.4	Discussion	34
4	One-dimensional structures in models with an area action	37
4.1	The surface model	38
4.1.1	Discretization of the surface model	40
4.2	Spikes and needles	43
4.2.1	The bosonic case	44
4.2.2	The supersymmetric case	46
4.2.3	Higher powers of the determinant	50
4.2.4	Higher dimensions	51

4.2.5	Exact solution for the tetrahedron	51
4.3	Simulations of the surface model	52
4.3.1	Observables	52
4.3.2	Implementation	54
4.3.3	Results	57
4.4	The matrix model	63
4.4.1	Needles in the matrix model	63
4.4.2	Simulations of the matrix model	64
4.5	Discussion	69
5	Summary	71

Chapter 1

Introduction

If we wanted to give a very general description of what we know about fundamental physics today, it would look something like this: There are four basic forces that shape the universe, namely electromagnetism, strong and weak interaction, and gravity. Each of these can individually be cast into a theoretical formalism that has been thoroughly tested and confirmed experimentally. Furthermore, electromagnetism, the weak interaction, and the strong interaction can all be joined in the more general formalism of the standard model of particle physics. The same, however, cannot be said about gravity.

Quantum theory and the theory of general relativity, even though they are both well tested in their respective areas of applicability, nevertheless seem to be incompatible with each other in a fundamental way that has so far defied all attempts to overcome the differences. This is not in itself a contradiction because the areas of applicability of both theories do not overlap, at least not in those parts of the universe that lend themselves to observation; generally speaking, quantum theory is important only on very small scales, whereas gravity effects are so weak that they can normally be observed only on very large scales. (In fact, gravity can be noticed at all only because, contrary to the other forces, it is both universally attractive and, by virtue of the graviton being massless, a long-range force.) This could be taken as a hint that both theories may be only effective models of a more general underlying theory that would consistently describe all four interactions. This theory, however, has yet to be found.

The problem is one that has been known for a long time, and the attempts to solve it are manifold. Invariably, however, given the inherent randomness of quantum theory and the equally inherent geometrical structure of general relativity, all these different approaches have one thing in common: they are all, in one way or another, theories of random geometries. In the models that will be of interest in this thesis, this fact manifests itself in a path integral over fluctuating spaces, described either by external coordinates (assuming a flat embedding space) or an internal metric. In particular, our focus will be on Euclidean quantum gravity, where the action of general relativity is put into a path integral, with the integration to be taken over

all possible metrics of a four-dimensional space-time; and on quantum string theory, where a path integral is taken over all possible world-sheets of the string.

However, the solution, and in some cases the very definition, of a path integral over surfaces is a difficult and mostly still unfinished problem. One reason is that any mathematical description of a surface, whether in terms of external or internal coordinates, is invariant under a reparametrization of these coordinates. This invariance has to be fixed in some way to ensure that only physically distinct surfaces are counted in the integral; unfortunately, there exists as yet no recipe for how to do this in three or more dimensions. In superstring theory, where the surfaces in question are two-dimensional, the path integral can be defined as an integral over the conformal factor, but it still cannot be solved except in an embedding space of dimension $d \leq 1$. Alternatively, superstrings can be studied in the critical dimension $d = 10$, where the surface integral decouples from the rest of the theory; however, one then has to find a way of arguing away the excess dimensions, a task that so far has not been conclusively solved, various compactification prescriptions notwithstanding.

A different possibility for treating an integral over metrics lies in trying to find an appropriate regularization. In particular, what we will be interested in is a discretization of the surfaces in question, *i. e.* we want to replace a continuous space-time or world-sheet with one built from finite elementary pieces. Such a discretization has already been attempted for both of the models in question; however, in both cases problems have emerged that prevent us from taking the model to a well-defined continuum limit. The aim of this thesis will be to examine possible modifications of these models in an attempt to improve their behaviour.

The remainder of this text is divided into four parts. The first of these is a general introduction to the practical issues of how to discretize an integral over metrics. Each of the following two parts deals with one of the mentioned models, respectively simplicial quantum gravity and quantum string theory. The results of both studies will be summarized in the final part.

Chapter 2

Dynamical triangulations

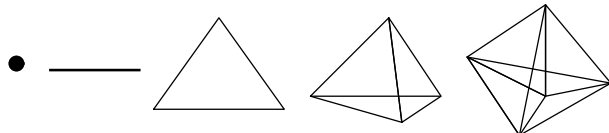
This chapter describes the basic techniques that will allow us to perform simulations of random geometries on a computer, independently of the actual model that we want to study. In principle, this is about taking an integration measure $\int \mathcal{D}g_{\mu\nu}$ over fluctuating metrics, discretizing it in terms of a fluctuating lattice, and putting it into a Monte Carlo algorithm. The integrand – *i.e.* the action, which holds the physical content of the model – will be inserted later.

2.1 Simplicial manifolds

First of all, we need to build the lattice itself, and define a metric on it. *A priori*, there is nothing to prevent us from choosing an ordinary hypercubic lattice [1]; in fact, simulations of random geometries can and have already been successfully performed in this way [2, 3]. However, for purposes of simulating models on fluctuating lattices, hypercubic structures are actually not the simplest possible choice. Instead, we are led to consider triangulations, lattices built from triangles or their higher-dimensional generalizations.

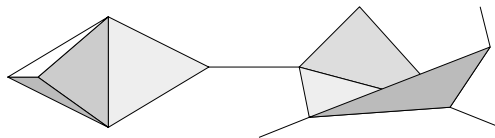
2.1.1 Definition of a simplicial manifold

Define a d -dimensional simplex or d -simplex $\langle i_1 \dots i_{d+1} \rangle$ as a set of $d+1$ points that are pairwise connected by links. Specifically, a 0-simplex $\langle i \rangle$ is defined as a single point or vertex; a 1-simplex $\langle ij \rangle$ is a line; a 2-simplex $\langle ijk \rangle$, a triangle; and a 3-simplex $\langle ijkl \rangle$, a tetrahedron. A 4-simplex $\langle ijklm \rangle$, the highest-dimensional construct we will be needing, is a four-dimensional analogue of the tetrahedron that can no longer be easily visualized.



Any subset $\langle i_{\alpha_1} \dots i_{\alpha_{k+1}} \rangle$ of vertices of a given d -simplex $\langle i_1 \dots i_{d+1} \rangle$, along with all connecting links between these vertices, forms a k -dimensional *subsimplex* or k -*subsimplex* of $\langle i_1 \dots i_{d+1} \rangle$. In particular, the $(d - 1)$ -subsimplices of a d -simplex are called its *faces*. Obviously, any d -simplex contains exactly $\binom{d+1}{k+1}$ k -subsimplices. In particular, a d -simplex always has $d + 1$ faces.

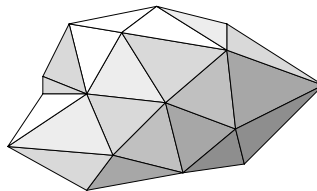
Two simplices are said to be *connected* if they share at least one subsimplex. We will be particularly interested in simplices that are connected by a common face, but in general any kind of connection is possible; we could join several tetrahedra at a common vertex, or even connect simplices of different dimensions, such as gluing a triangle to a tetrahedron so that they share a common link. Any set of connected simplices is called a *simplicial complex*.



In principle, a simplicial complex is already serviceable as a lattice; at any rate, we can define fields and derivatives on it [4]. However, it does not bear much resemblance to any kind of physical space; in particular, we can in most cases not even assign a dimension to it. If we want a simplicial complex to function as the discrete analogue to some d -dimensional space, we need to impose some sort of manifold condition.

To this end, first define the d -dimensional *neighbourhood* of a given subsimplex $\langle i_1 \dots i_{k+1} \rangle$ as the set of all d -simplices that contain $\langle i_1 \dots i_{k+1} \rangle$. For example, on a tetrahedron the two-dimensional neighbourhood of a vertex consists of the three triangles that meet at this vertex, while its three-dimensional neighbourhood is just the tetrahedron itself. The size of the highest-dimensional neighbourhood that exists around a given subsimplex is called that subsimplex's *order* $o_{i_1 \dots i_{k+1}}$.

With this, we can now define a d -dimensional *simplicial manifold* or *triangulation*, in analogy to a continuum manifold, as a simplicial complex S with the additional requirement that the d -dimensional neighbourhood of any vertex $\langle i \rangle \in S$ be homeomorphic to a d -dimensional ball.



In $d \leq 2$ dimensions, this condition can be fulfilled simply by taking a number of d -simplices and gluing them together along their faces in such a way that each face belongs to exactly two d -simplices. In more than two dimensions, this process in general creates only a *pseudo-manifold*, where not every vertex's neighbourhood is homeomorphic to a ball. Fortunately, however, the method by which we will create

configurations in the numerical algorithm is guaranteed to produce actual simplicial manifolds as long as we can provide a starting configuration of this kind.

2.1.2 The discrete metric

Once we know how to build the lattice, the next step is to define a metric on it in such a way that we can choose a well-defined integration measure $\mathcal{D}g_{\mu\nu}$. Usually, this is done by demanding the following:

- The metric is flat inside the d -simplices.
- The metric remains continuous when moving from one d -simplex to another by crossing a face.
- The faces are flat linear subspaces of the d -simplices that contain them.

In this way, the curvature on the lattice can be non-zero only in the $(d - 2)$ -subsimplices – the vertices on a two-dimensional triangulation, or the triangles in $d = 4$. Such a metric is called, for obvious reasons, *piecewise flat*.

The integration measure

What, now, remains of an integral over metrics in such a piecewise flat space? In principle, there are still two things whose variation can change the metric: the connectivity of the simplices, and the lengths of the links. In general, we would therefore replace the integral over metrics by a sum over triangulations and an integral over link lengths,

$$\int \mathcal{D}g_{\mu\nu} \rightarrow \sum_T W(T) \prod_{\langle ij \rangle} \mathcal{D}l_{ij} \quad (2.1)$$

where the weights $W(T)$ and the measure $\mathcal{D}l_{ij}$ have still to be defined.

In practice, one does not actually use the general form (2.1), but restricts oneself to varying either the connectivity or the link lengths. The latter method, integration over link lengths on a fixed triangulated lattice, is the one closest to the original idea by Regge [5], and is therefore known as *Regge calculus*, or alternatively *fixed triangulations*.¹ Unfortunately, it has a number of problems; among other things, reparametrization invariance is still a serious difficulty in the choice of the measure $\mathcal{D}l_{ij}$, and so far, all attempts to apply Regge calculus to two-dimensional simplicial quantum gravity have produced results that are in variance to those of the analytic solution of the continuum theory that exists in this case [7, 8].

The other method, and the one we will use here, is called *dynamical triangulations* [9, 10, 11] and consists of summing over all possible connectivities while keeping all

¹It should be mentioned that Regge suggested this method as a way of treating classical gravity only; the idea of using it to regularize a path integral over fluctuating surfaces was not formed until much later [6].

link lengths fixed and, for simplicity, equal to each other. This leaves us with the responsibility of deciding on the weights $W(T)$, which have to be chosen in such a way as to avoid any overcounting of equivalent configurations due to reparametrizations. Fortunately, any two different connectivities automatically represent physically distinct metrics [12], so the only thing we have to worry about is the possible existence of different parametrizations of the same connectivity.

This possibility depends on exactly how we describe a triangulation. If we use *labeled triangulations*, where each vertex, link, triangle, and so on gets a specific ‘name’ attached to it, then the number of different possible descriptions of a given connectivity is $n_0!n_1!\dots n_d!$, where n_i is the number of i -simplices on the triangulation. Each of these labelings can be thought of as a different parametrization of the same geometrical structure, and we would therefore divide out the number of all possible labelings in the sum over triangulations; in other words, for labeled triangulations we would choose the weights as $W(T) = \frac{1}{n_0!n_1!\dots n_d!}$.

Many possible labelings of a given connectivity can be mapped onto each other by a permutation of their labels, which means that they all correspond to the same *unlabeled* configuration. In fact, one might naively assume that there should be exactly one unlabeled configuration for each distinct connectivity, giving us a constant factor of $n_0!n_1!\dots n_d!$ between labeled and unlabeled triangulations. However, this is true only if the configuration is not symmetric. If there exist two vertices that are both connected to exactly the same neighbouring vertices, then these two can be exchanged without altering the connectivity; but the exchange still gives us a new unlabeled configuration, because now we are actually exchanging vertices and not just labels. In general, if we denote the number of possible vertex exchanges by the *symmetry factor* $C(T)$, with $C(T) = 1$ for a completely non-symmetric configuration, we can write the number of labeled configurations that correspond to the same unlabeled one as $\frac{n_0!n_1!\dots n_d!}{C(T)}$. Thus, we would for unlabeled triangulations change the weights to $W(T) = \frac{1}{n_0!n_1!\dots n_d!} \frac{n_0!n_1!\dots n_d!}{C(T)} = \frac{1}{C(T)}$.

Since all we really care about is the geometrical structure of a configuration and not some arbitrary choice of labels, we will use unlabeled triangulations.² Our discretization prescription for an integral over metrics should therefore be

$$\int \mathcal{D}g_{\mu\nu} \rightarrow \sum_T \frac{1}{C(T)} \quad (2.2)$$

So far, we have not yet specified which set of triangulations \mathcal{T} we intend to use. Trying to actually sum over *all* triangulations, including all possible topologies, does not seem feasible because the number of distinct triangulations is estimated to grow factorially with the number of simplices, whereas we cannot expect the action, in any interesting model, to provide more than an exponential suppression of configurations. To obtain a well-defined sum over triangulations we should therefore restrict ourselves

²This might appear inconsistent with the fact that I use sets of labels $\langle i_1 \dots i_{d+1} \rangle$ to represent simplices. However, this is only a convenience of notation. It is always implied that any different labeling of the same simplex is to be regarded as equivalent.

to a set that is at least exponentially bounded. This seems to be the case if we restrict ourselves to just one topology [13]. We will again go for the simplest case first and study only configurations with spherical topology (no ‘holes’). For simulations of models with different topologies, see for example [14, 15].

Of course, it should be clear from the preceding discussion that the substitution (2.2) is not the only possible discretization of an integral over metrics, nor have we shown yet that it is actually a good one. For example, we do not know whether our chosen set of discrete metrics really provides us with a good representation of the complete space of continuous metrics. For now, we simply deal with a particular discrete model, and still have to show that it reproduces the original theory in a suitable continuum limit. Justification for the hope that this might indeed be the case comes mainly from simulations of two-dimensional simplicial quantum gravity, where both the continuum model and the triangulated version can be solved analytically, and the results shown to agree with each other. More on this in chapter 3.

2.2 Numerical simulations

Even though the replacement of the integral over metrics by a sum over triangulations greatly simplifies matters, it is in most cases still not enough for an analytic treatment of the model in question. Instead, numerical methods are used to extract information about it. In this section, I will shortly describe the basics of the Monte Carlo algorithm in general, and its application to triangulations in particular.

2.2.1 Monte Carlo algorithms

Generally speaking, a Monte Carlo simulation is a numerical method for estimating the value of an integral, typically with many degrees of freedom, that cannot be solved exactly. In its simplest version, it consists of randomly sampling the integration space, evaluating the function in question in the chosen points, and using the average of these values as an approximation for the real integral. In other words, we estimate an integral of some function f over an integration space I by

$$\frac{1}{A} \int_I d^d x f(x) \approx \frac{1}{N(I_0)} \sum_{x \in I_0} f(x) \quad (2.3)$$

where I_0 is the random sample of the integration space, $N(I_0)$ is the number of points in this sample, and $A \equiv \int_I d^d x$ is the volume of the integration space (assuming, of course, that it is finite).

Using this formula on the special case of a discrete sum over triangulations weighted with an action $S(T)$ gives us

$$\frac{1}{N(\mathcal{T})} \sum_{T \in \mathcal{T}} e^{-S(T)} \approx \frac{1}{N(\mathcal{T}_0)} \sum_{T \in \mathcal{T}_0} e^{-S(T)} \quad (2.4)$$

Likewise, we can estimate the expectation value of some observable \mathcal{O} as

$$\langle \mathcal{O} \rangle \equiv \frac{\sum_{T \in \mathcal{T}} \mathcal{O}(T) e^{-S(T)}}{\sum_{T \in \mathcal{T}} e^{-S(T)}} \approx \frac{\sum_{T \in \mathcal{T}_0} \mathcal{O}(T) e^{-S(T)}}{\sum_{T \in \mathcal{T}_0} e^{-S(T)}} \quad (2.5)$$

where $N(\mathcal{T})$ and $N(\mathcal{T}_0)$ drop out because of the normalization factors.

Importance sampling

So far, we have assumed that the random sample is chosen from a flat distribution, *i. e.* each point in the configuration space is picked up with equal possibility. While this is a valid approach that eventually leads to correct results, it also tends to produce large statistical errors, especially if we have an exponential weight as in (2.5). In this case, only a small part of the configuration space is actually significant for the result, which means that the algorithm will pick up unimportant configurations almost all of the time, leading to extremely long simulation times.

The way around this is to pick each configuration not from a flat distribution, but with a probability that is given by its weight, $p(T) \sim e^{-S(T)}$. This ensures that those configurations that contribute the most to the overall sum are also the most likely to be picked, whereas configurations with a weight near zero will be ignored most of the time. The estimate of an observable's expectation value $\langle \mathcal{O} \rangle$ simplifies in this case to

$$\langle \mathcal{O} \rangle \approx \frac{1}{N(\mathcal{T}_0)} \sum_{T \in \mathcal{T}_0} \mathcal{O}(T) \quad (2.6)$$

However, even for an only moderately complicated action it is in general not possible to simply generate this distribution. What can be done instead is to choose configurations from a *Markov chain* that has $p(T)$ as its static distribution.

A Markov chain describes the evolution of a statistical model whose state at any given point t in the chain depends only on its state at the previous point, $t-1$. Thus, a Markov chain is fully characterized by a set of transition probabilities $P(A \rightarrow B)$ for all pairs of configurations (A, B) , plus a set of starting probabilities $p(A)$. We also demand that the following three conditions be fulfilled:

- The chain is *irreducible*. This means that if we denote by $P^i(A \rightarrow B)$ the probability of the chain reaching a configuration B from A in exactly i steps, then there exists for any pair of configurations (A, B) a finite i such that $P^i(A \rightarrow B) > 0$.
- The chain is *aperiodic*. This means that for any configuration A and any finite number i , there exists a non-vanishing probability of the chain returning to A after exactly i steps, $P^i(A \rightarrow A) > 0$.

- The transition probabilities are *stationary*. This means that there exists a probability distribution π such that

$$\sum_A \pi(A)P(A \rightarrow B) = \pi(B) \quad (2.7)$$

is true for all configurations B .

If this is assured, it can be shown that the i -step transition probabilities $P^i(A \rightarrow B)$ converge to the stationary distribution $\pi(B)$ independently from where we start,

$$\lim_{i \rightarrow \infty} P^i(A \rightarrow B) = \pi(B) \quad \forall A \quad (2.8)$$

Thus, coming back to our specific task, we can use a Markov chain to create a set of randomly chosen configurations A weighted by $e^{-S(A)}$ if we can just choose the transformation probabilities $P(A \rightarrow B)$ in such a way that we have a stationary distribution $\pi(A) \sim e^{-S(A)}$. A sufficient condition for this can be found in the *detailed balance equation*

$$\pi(A)P(A \rightarrow B) = \pi(B)P(B \rightarrow A) \quad (2.9)$$

which implies (2.7), as can be seen by taking the sum over all A on both sides.

One possible choice of $P(A \rightarrow B)$ that fulfils (2.9) is the following:

$$P(A \rightarrow B) = \min \left(1, \frac{\pi(B)}{\pi(A)} \right) = \min \left(1, e^{S(A)-S(B)} \right) \quad (2.10)$$

The Metropolis algorithm

To summarize, we now have the following recipe for ‘measuring’ the expectation value of an observable \mathcal{O} in a given triangulated model:

1. Choose an arbitrary triangulation as a starting point.
2. Propose a random transformation to a different triangulation; accept or reject it with a probability given by (2.10). Repeat this step sufficiently often so that the chain comes close to its stationary distribution.³
3. Calculate \mathcal{O} .
4. Repeat steps 2 and 3 until we have a reasonably large sample to estimate $\langle \mathcal{O} \rangle$.

This procedure is known as the *Metropolis algorithm*.

³How do we know what ‘sufficiently often’ means? There is no mathematically exact criterion for this, but we can give a good estimate of the required number of steps by measuring the integrated autocorrelation time τ while running the simulation. If we perform a number of transformations equal to a few times τ , we can be reasonably confident that any dependence on the starting configuration is gone, which in turn can be taken to mean that we have come close enough to the stationary distribution.

2.2.2 Transformations

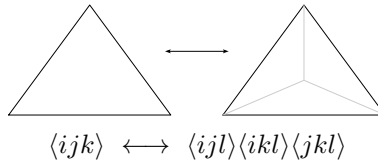
The one thing we still need to implement a simulation of dynamical triangulations is a set of transformations that change the connectivity of the simplices. It is clear from the discussion above that to be of any use in a Metropolis algorithm, this set has to be *ergodic*, *i. e.* it must be possible to reach any configuration from any other by applying a finite number of these transformations. From a purely practical viewpoint, we would also like this set to be as small and simple as possible.

The transformations that are best suited to these purposes are the so-called (p, q) moves. Their general definition is the following: On a d -dimensional simplicial manifold, choose p d -simplices that are connected to each other in such a way that they form part of a d -dimensional minimal sphere. (A minimal sphere is the smallest possible simplicial manifold of a given dimension; it consists of $d+1$ simplices that are pairwise connected by a face, so that they form the surface of a $(d+1)$ -simplex. For example, a two-dimensional minimal sphere is the surface of a tetrahedron.) Then replace this complex by the $q = d - p + 2$ simplices that would complete the minimal sphere. Obviously, in this way one arrives at $d + 1$ different possible moves, which together can be shown to be ergodic, at least in dimensions $d \leq 4$ [16].⁴ Note that move (p, q) is the inverse of (q, p) , *i. e.* using move (q, p) on exactly those simplices created by move (p, q) leads back to the original configuration.

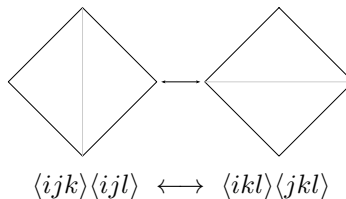
To better illustrate this rather abstract definition, here is what the (p, q) moves look like in detail in the cases that interest us, namely two and four dimensions.

The (p, q) moves in two dimensions

In $2d$, we have three moves: $(1, 3)$, $(2, 2)$, and $(3, 1)$.



$(1, 3)$: Take any triangle, insert a new vertex in its centre, and connect this point to all the vertices on the triangle. This creates three new triangles, while the original one is removed from the configuration. $(3, 1)$: The reverse of $(1, 3)$; take three triangles that share a common vertex of order 3, then remove this vertex and all links connected with it, thus replacing the three triangles with one new 2-simplex.



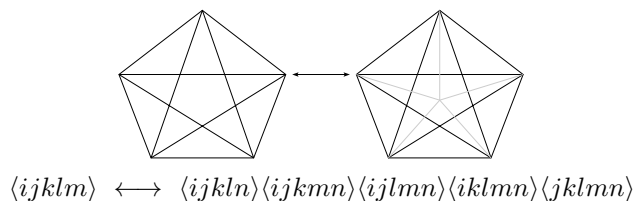
⁴The actual proof is rather long and depends on showing the equivalence of (p, q) moves with another kind of transformations called Alexander moves that are known to be ergodic [17].

(2, 2): Take two triangles that share a common link, remove this link, and replace it with a new one connecting the other two vertices. This move is its own inverse. Note that in a canonical ensemble of two-dimensional triangulations, this move is ergodic by itself, *i. e.* we can reach any configuration with n_2 triangles from any other that has the same number of triangles by repeated application of move (2, 2) only [11, 18].

Move (2, 2) is also the first case where we encounter the phenomenon of so-called *degenerate manifolds*, meaning configurations where two different simplices or sub-simplices are built from the same set of vertices, *i. e.* lying on top of each other. In this particular case, it is possible that the two vertices being connected already do have a link in common, so that after the move they would be connected by two different links. While this is not necessarily a problem – simulations including degenerate manifolds can and have been performed, and apparently lead to similar results [19, 20] – we would nevertheless like to avoid these configurations. This means that before performing this move, we have to check whether there already exists a link connecting the two vertices in question; if so, the move has to be rejected by the algorithm.

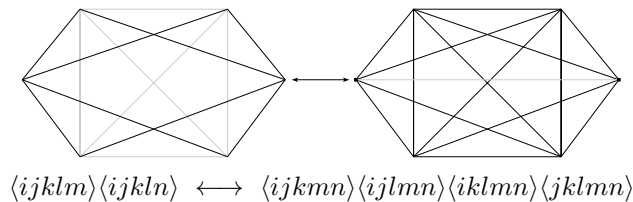
The (p, q) moves in four dimensions

In $4d$, we have five moves. These are somewhat harder to illustrate than their two-dimensional counterparts, but the analogies should be obvious.



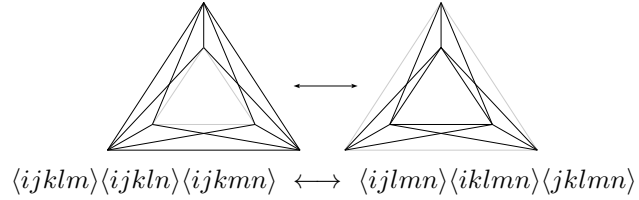
(1, 5): Choose a 4-simplex, insert a new vertex in its centre, and connect it with the other vertices, thus destroying the original 4-simplex and creating five new ones.

(5, 1): The inverse of this, where we take five 4-simplices joined at a vertex of order 5 and remove this vertex, thus destroying five 4-simplices and creating one.



(2, 4): Choose two 4-simplices that have a common face, take the two vertices that are not part of this face, and connect them by a link. This destroys the original 4-simplices (and thus also the tetrahedron that formed their common face) and creates four new ones. With this move, we again have to test for a double link to avoid creating a degenerate configuration. (4, 2): The inverse, where we choose

four 4-simplices joined at a link of order 4, remove the link, and replace it by a tetrahedron joining two new 4-simplices. Again, we have to test whether there is already a tetrahedron present that contains the same four vertices.



(3, 3): Choose three 4-simplices that share a common triangle of order 3, remove this triangle, and create a new one from the three vertices that were not part of the original triangle. This also destroys the original three 4-simplices and creates three new ones. Again, we have to test for the presence of a triangle in the place where we are trying to create the new one. Like (2, 2), this move is its own inverse.

Chapter 3

The strong coupling expansion in simplicial quantum gravity

Simplicial quantum gravity is an attempt to quantize Einstein's theory by taking a path integral over all physically distinct d -dimensional Riemannian surfaces, weighted with the Einstein-Hilbert action of general relativity. Given the inherent difficulties of defining such an integral over fluctuating geometries, the model is then discretized by means of dynamical triangulations in an attempt to make sense of it. This approach can be directly shown to be valid in $d = 2$ dimensions, which gives us hope that it might be made to work in the physically interesting case of $d = 4$ dimensions as well. The situation is more complicated there, however, and as I will show there are reasons to believe that the addition of matter fields could be essential for the four-dimensional model to work.

The aim of this chapter is twofold. For one thing, we want to introduce an alternative method for the evaluation of the partition function, namely the strong coupling expansion. This method has already been used in the context of two-dimensional simplicial quantum gravity [49, 50], but has to be adapted to work in the more complicated case of four dimensions. Secondly, we want to apply this method to study the changes in the model if it is coupled to matter fields. Also, I will compare the results of the strong coupling expansion to those found in Monte Carlo studies of the same model.

3.1 Simplicial quantum gravity

The equations of motion of general relativity are

$$R_{\mu\nu} - g_{\mu\nu} \left(\frac{1}{2} R - \lambda \right) = 8\pi G T_{\mu\nu} \quad (3.1)$$

where $g_{\mu\nu}$ is the metric tensor, $R_{\mu\nu}$ is the Ricci tensor, $R \equiv R^\mu{}_\mu$ is the scalar curvature, $T_{\mu\nu}$ is the energy-momentum tensor, λ is the cosmological constant, and G is Newton's constant.

These equations can be derived from the action principle using the Einstein-Hilbert action

$$S_{EH} = \frac{1}{8\pi G} \int d^d x \sqrt{-|g|} \left(\frac{1}{2} R - \lambda \right) + S_{matter} \quad (3.2)$$

where S_{matter} is the action for the matter fields, $|g|$ is the determinant of the metric tensor, and d is the dimensionality of space-time. (Obviously, to describe our physical universe we should set $d = 4$, but in principle the model can be defined in any dimension; as we will see, we can learn much about the dynamics of the four-dimensional model by studying the two-dimensional one first.)

We can try to quantize this theory by taking the path integral

$$Z = \int \mathcal{D}g_{\mu\nu} e^{-iS_{EH}} \quad (3.3)$$

where the integration is to be performed over all physically distinct metrics with given boundary conditions. As written, this is for now just a formal expression; even disregarding the question of how to define the integration measure, we find that we have some difficulties to deal with.

For one thing, we see that for a Lorentzian space-time – where the metric has a signature $(-+++)$ – the Einstein-Hilbert action (3.2) is real, making the integrand of (3.3) oscillatory and thus in general rendering the integral ill-defined [21]. This problem is not unique to the model discussed here; it is well-known in quantum field theory, where it can be dealt with by performing a Wick rotation on the metric, replacing the time coordinate by an imaginary quantity $t \rightarrow -i\tau$ and thus giving the metric a Riemannian signature $(++++)$. In our case, this would result in the following modified versions of the Einstein-Hilbert action

$$S_{EH} = -\frac{1}{8\pi G} \int d^d x \sqrt{|g|} \left(\frac{1}{2} R - \lambda \right) + S_{matter} \quad (3.4)$$

and the path integral

$$Z = \int \mathcal{D}g_{\mu\nu} e^{-S_{EH}} \quad (3.5)$$

This ansatz is commonly called ‘Euclidean’ quantum gravity, even though ‘Riemannian’ would be more accurate. One can hope that once a solution to the Euclidean model has been found, it might be possible to continue it analytically into the region of Lorentzian metrics. An example of a case where this method apparently works comes from semi-classical calculations of the spectrum of Hawking radiation [22], where a treatment of the model in both the Euclidean and the Lorentzian sector leads to exactly the same thermal radiation distribution [23].

Even if we accept the Wick rotation as valid, however, we are immediately confronted with a new problem, namely that the action (3.4) is not positive definite; in fact, we can make it arbitrarily large and negative just by choosing a suitably

extreme curvature, and thus cause the path integral to blow up. There is no obvious cure for this problem, and it therefore seems that, even if we knew how to choose the measure $\mathcal{D}g_{\mu\nu}$, the integral would still have to be regularized in some way.

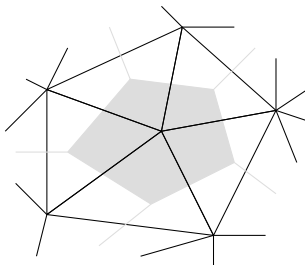
In this situation, a discretization in terms of dynamical triangulations looks very promising, since it not only provides us with a definition of the measure but also, by way of the fixed link lengths, introduces an upper limit on the curvature, which in turn makes the action bounded from below.¹ The crucial question, of course, is whether it is possible to take the resulting model to a continuum limit in which the original theory is recovered.

3.1.1 Discretization of pure gravity

We will start with a discussion of the model without matter fields, $T_{\mu\nu} = 0$ (‘pure gravity’). Since we already know how we want to discretize the integral over metrics, all that remains to be done is to find the discrete version of the action. This was first done in [26, 27]; here I will only briefly describe the necessary steps.

The curvature on a simplicial manifold

First, we need a definition of curvature on a d -dimensional triangulation. From our choice of the discrete metric, we know that the curvature can exist only on the $(d-2)$ -subsimplices. For each of these subsimplices $\langle i_1 \dots i_{d-1} \rangle$ we can define $R_{i_1 \dots i_{d-1}}$, in analogy to the continuum definition, as the change of direction of a vector after parallel transport around an area that includes the subsimplex itself but no others. The generic choice for such an area is the *dual polygon* of $\langle i_1 \dots i_{d-1} \rangle$, which can be found by going around the subsimplex and connecting the centres of all d -simplices in its neighbourhood.



The dual polygon of a vertex on a two-dimensional simplicial manifold.

The change of direction of a vector is then given by the deficit angle

$$\delta_{i_1 \dots i_{d-1}} = 2\pi - \sum_{jk: \langle i_1 \dots i_{d-1} jk \rangle} \theta_{i_1 \dots i_{d-1} k}^{i_1 \dots i_{d-1} j} \quad (3.6)$$

¹One might worry about the effects of an artificial bound like this on the results of numerical simulations of the model, since it might seem that the system should simply stick to the upper limit and thus prevent us from observing the model’s dynamics. However, it was shown that this is actually not the case [24, 25]. Specifically, it was found that the distribution of the integrated curvature exhibits a peak that is near to but still clearly below the upper bound.

where $\theta_{i_1 \dots i_{d-1} j}$ is the dihedral angle formed by the two faces $\langle i_1 \dots i_{d-1} j \rangle$ and $\langle i_1 \dots i_{d-1} k \rangle$.

For the special case of dynamical triangulations, this formula becomes particularly simple: because all links are of equal length, the angle between two faces of a simplex is just a constant, $\theta_d \equiv \arccos 1/d$, and we have

$$\delta_{i_1 \dots i_{d-1}} = 2\pi - \sum_{jk: \langle i_1 \dots i_{d-1} jk \rangle} \theta_d = 2\pi - \theta_d o_{i_1 \dots i_{d-1}} \quad (3.7)$$

where $o_{i_1 \dots i_{d-1}}$ is the order of $\langle i_1 \dots i_{d-1} \rangle$ as defined in section 2.1.1. Accordingly, the curvature of a $(d-2)$ -subsimplex can be defined as

$$R_{i_1 \dots i_{d-1}} \equiv \frac{2\pi - \theta_d o_{i_1 \dots i_{d-1}}}{V_{i_1 \dots i_{d-1}}^{dual}} \quad (3.8)$$

where $V_{i_1 \dots i_{d-1}}^{dual}$ is the volume of the dual polygon. Note that in two dimensions we have $\theta_2 = \pi/3$, which gives us $R_{i_1 \dots i_{d-1}} = 0$ whenever $o_{i_1 \dots i_{d-1}} = 6$, *i.e.* a two-dimensional triangulation is locally flat around any vertex of order 6. This is consistent with the well-known fact that we can completely fill a flat plain with regular hexagons. In four dimensions, we find an angle $\theta_4 = 1.318116\dots$ that is not an integer divisor of 2π , which means that it is impossible to make a four-dimensional triangulation locally flat. However, we can still have triangulations that are almost flat, if the average triangle order is equal to $2\pi/\theta_4$ and the variance is small.

The partition function of simplicial quantum gravity

Now all the necessary tools for discretizing the integral (3.5) are assembled; we just have to put the building blocks together. We replace

$$\int d^d x \sqrt{g} R \rightarrow \sum_{\langle i_1 \dots i_{d-1} \rangle} V_{i_1 \dots i_{d-1}}^{dual} \frac{2\pi - \theta_d o_{i_1 \dots i_{d-1}}}{V_{i_1 \dots i_{d-1}}^{dual}} = 2\pi n_{d-2} - \theta_d \frac{d(d+1)}{2} n_d \quad (3.9)$$

$$\int d^d x \sqrt{g} \lambda \rightarrow \sum_{\langle i_1 \dots i_{d+1} \rangle} V_{i_1 \dots i_{d+1}} \lambda = V_d \lambda n_d \quad (3.10)$$

$$\int \mathcal{D}g_{\mu\nu} \rightarrow \sum_T \frac{1}{C(T)} \quad (3.11)$$

where in (3.9) we used the fact that every d -simplex has a number of $(d-2)$ -simplices equal to $\binom{d+1}{d-1} = \frac{d(d+1)}{2}$, so that

$$\sum_{\langle i_1 \dots i_{d-1} \rangle} o_{i_1 \dots i_{d-1}} = \frac{d(d+1)}{2} n_d \quad (3.12)$$

and in (3.10) we noted that on dynamical triangulations every d -simplex has a fixed volume that we denote by V_d .

All in all, we find as the partition function of pure simplicial quantum gravity in d dimensions

$$Z(\kappa_d, \kappa_{d-2}) = \sum_T \frac{1}{C(T)} e^{\kappa_{d-2} n_{d-2} - \kappa_d n_d} \quad (3.13)$$

where $\kappa_{d-2} \sim \frac{1}{G}$ and $\kappa_d \sim \frac{\lambda + \text{const.}}{G}$ are the discrete versions of the model's two coupling constants. Alternatively, we can also consider the canonical partition function

$$Z(n_d, \kappa_{d-2}) = \sum_T \frac{1}{C(T)} e^{\kappa_{d-2} n_{d-2}} \quad (3.14)$$

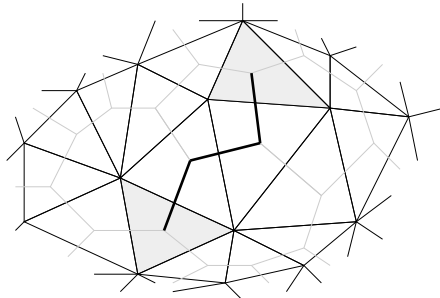
where the sum now runs over all triangulations of a given size n_d .

3.1.2 The structure of space-time

Before going on to discuss the properties of (3.13), we first need to define some suitable observables that we can use to describe the overall ‘shape’ of a given space-time.²

The Hausdorff dimension

One way of describing the ‘real’ dimensionality of space-time (as opposed to the canonical dimension d) is by the *fractal dimension* or *Hausdorff dimension* d_H . To define it on a simplicial manifold, we first need some concept of geodesic distance between simplices. For two d -simplices $\langle i_1 \dots i_{d+1} \rangle$ and $\langle j_1 \dots j_{d+1} \rangle$, define $d_{j_1 \dots j_{d+1}}^{i_1 \dots i_{d+1}}$ as the length (number of links) of the shortest path that connects the two simplices on the dual lattice (the lattice formed by the dual polygons of all d -simplices on the triangulation).



Two triangles at distance 3 from each other.

²I should note that using the word ‘space-time’ to describe a manifold with Riemannian signature is of course something of a misnomer, since there is no direction that could be identified as a time coordinate. Nevertheless, I will continue to refer to it as such, since a four-dimensional space-time is what we are ultimately trying to represent.

Next define a d -dimensional sphere of radius r around a simplex $\langle i_1 \dots i_{d+1} \rangle$ as the set of all d -simplices whose geodesic distance from the center is less than or equal to r ,

$$S_{i_1 \dots i_{d+1}}^r \equiv \left\{ \langle j_1 \dots j_{d+1} \rangle : d_{j_1 \dots j_{d+1}}^{i_1 \dots i_{d+1}} \leq r \right\} \quad (3.15)$$

The Hausdorff dimension is now defined by the relation between the volume of a d -dimensional sphere (which is, of course, proportional to the number of simplices contained in it) and its radius,

$$V \sim r^{d_H} \quad (3.16)$$

For a smooth space-time, $d_H = d$, but in a fractal universe, d_H can be very different from the canonical dimension. It is not entirely clear what we should expect from a sensible model of quantum gravity – obviously, we should have $d_H = 4$ at large scales, since that is what we can observe in our universe; but at small scales, quantum effects could very well change d_H . If so, however, it seems reasonable that they should make space-time more fractal, not less, so a measured value of $d_H < 4$ can probably be regarded as a bad sign.

The string susceptibility exponent

The other observable that we will be most interested in is the *string susceptibility exponent* γ , which describes the singular behaviour of the grand-canonical partition function,

$$Z(\kappa_d, \kappa_{d-2}) \sim Z_{analytic}(\kappa_d, \kappa_{d-2}) + (\kappa_d - \kappa_d^c)^{2-\gamma} + \text{less singular terms} \quad (3.17)$$

where the critical value of κ_d is in two dimensions a constant, whereas in four dimensions it depends, as a monotonously increasing function, on the choice of the other coupling constant, $\kappa_d^c = \kappa_d^c(\kappa_{d-2})$. If the susceptibility exponent exists (*i. e.* if $|\gamma| < \infty$), then (3.17) implies an asymptotic behaviour of the canonical partition function

$$Z(n_d, \kappa_{d-2}) \sim e^{\kappa_d^c n_d} n_d^{\gamma-3} \quad (3.18)$$

The maximal value of the susceptibility exponent that can be expected is $\gamma = \frac{1}{2}$, which corresponds to a sort of mean field value and describes surfaces shaped like branched polymers (see below). Furthermore, there exists a theorem [28, 29] saying that any value of $\gamma > 0$ automatically implies $\gamma = 1/2$.³ Therefore, we would for a physical space-time expect to find $\gamma \leq 0$.

³This theorem was later shown to have a few loopholes, but the only alternatives to $\gamma = 1/2$ discovered so far are likewise uninteresting [30].

3.1.3 The two-dimensional case

Now that we have the necessary tools, we can proceed to a discussion of the properties of the model (3.13). I will first give a brief overview of the situation in two dimensions, where the model simplifies considerably, and actually becomes analytically solvable.

For one thing, the Einstein-Hilbert action in this model becomes a topological invariant, courtesy of the Gauss-Bonnet theorem which tells us that on any two-dimensional simplicial manifold we have

$$\int d^2x \sqrt{|g|} R = 4\pi (1 - h) \quad (3.19)$$

where h is the genus (number of holes) of the manifold.⁴ Among other things, this means that the action is no longer unbounded from below.

The other big simplification in two dimensions is that the metric tensor, due to reparametrization invariance and its own symmetry, has only one independent parameter left.⁵ This means that we can choose to write it in the *conformal gauge*

$$g_{\mu\nu}(x) \equiv \hat{g}_{\mu\nu} e^{\Phi(x)} \quad (3.20)$$

where the $\hat{g}_{\mu\nu}$ are constants, and integrate only over the field Φ . The resulting model is known as *Liouville theory*.

The string susceptibility exponent in this model can be calculated analytically, and comes out as $\gamma = -\frac{1}{2}$. What is more, we can even generalize the model by including various types and numbers of (conformally invariant) matter fields, and still get an exact value of γ . As it turns out, this value depends only on the central charge c of these fields. The calculation can be performed for all $c \leq 1$, and yields [31, 32, 33]

$$\gamma = \frac{1}{12} \left(c - 1 - \sqrt{(c - 25)(c - 1)} \right) \quad (3.21)$$

This behaviour is known as *KPZ scaling*, and for as long as it applies, the model is said to be in the *Liouville phase*.

Beyond the so-called ‘ $c = 1$ barrier’, the formula (3.21) breaks down, and we leave the Liouville phase to enter a regime where the fractal structure of the universe degenerates into that of a branched polymer: a tree structure that is built from many long but very thin tubes, with a susceptibility exponent $\gamma = \frac{1}{2}$ and a Hausdorff dimension $d_H = 2$. This structure can be explained as the condensation of so-called ‘spikes’; the free energy of a spike can be estimated from the effective action for the conformal factor as [34, 35, 36]

$$F_{spike} \sim (1 - c) \ln \frac{l}{a} \quad (3.22)$$

⁴Of course, this means that classically the model becomes trivial, since Einstein’s equations will be automatically fulfilled. However, as we will see the path integral (3.5) nevertheless has non-trivial properties due to quantum effects.

⁵More precisely, this is true only if the metric is not singular.

where l is the length of the spike and a is a cut-off length introduced to prevent singularities of the metric. Obviously, for $c > 1$ F_{spike} can become arbitrarily large and negative if we just take a sufficiently long spike. It therefore seems clear that this, the *elongated phase* or *branched polymer phase*, is physically meaningless; apparently, a well-defined theory of two-dimensional Euclidean quantum gravity can exist only if it does not contain ‘too much’ matter.

If we now look at the discretized version of the model, we find that it, too, simplifies to the point where an analytic treatment is possible. On a two-dimensional simplicial manifold with a fixed number of triangles, the number of vertices is a topological invariant, $n_0 = \frac{1}{2}n_2 + 2 - 2h$, a convenience that is no longer available in higher dimensions. As a result, we find in analogy to the Gauss-Bonnet theorem that the total curvature becomes once more a constant,

$$\sum_{\langle i \rangle} V_i^{dual} R_i = 2\pi n_0 - \pi n_2 = 4\pi(1 - h) \quad (3.23)$$

The resulting model can be shown to be equivalent to a solvable one-matrix model [4]. More specifically, the dual graph of each two-dimensional triangulation with n_2 triangles can be interpreted as the Feynman diagram belonging to a term of order n_2 in the matrix model’s series expansion, and vice versa.

The solution of this matrix model, when taken to its planar limit, shows that the two-dimensional triangulated model does indeed have a critical point where a continuum limit can be constructed. At this point, one also finds a string susceptibility exponent $\gamma = -\frac{1}{2}$, which agrees with the pure gravity value found in Liouville theory.

Finally, we can of course also perform numerical simulations of the discretized model. This has been done both for pure gravity and for various values of $c \neq 0$, as well as for a modified partition function where an additional factor $\prod_{\langle i \rangle} o_i^\beta$ is included. This extra factor will be discussed in detail later; for now, we can just regard it as the result of a slightly different discretization procedure. The results of the simulations are indeed found to agree with the analytic calculations (in those cases where the calculations can be performed); from them, we can construct a phase structure as depicted in figure 3.1.

As we can see, both the Liouville phase and the branched polymer phase of pure gravity are reproduced for the appropriate values of c . Apart from that, we see that by a combination of sufficiently extreme values of c and β we can drive the system into a third phase. In this, the *collapsed phase*, the geometry of the discretized model degenerates to what is often called ‘pancake configurations’: two of the vertices become *singular* in the sense of developing an order that grows linearly with the volume of the triangulations, so that almost all other vertices are connected to these two. The result is a universe that is basically a compressed disc, with an extremely large negative curvature (tending towards infinity with growing n_2) in the two singular vertices; it seems clear that this phase is of no more physical relevance than branched polymers are.

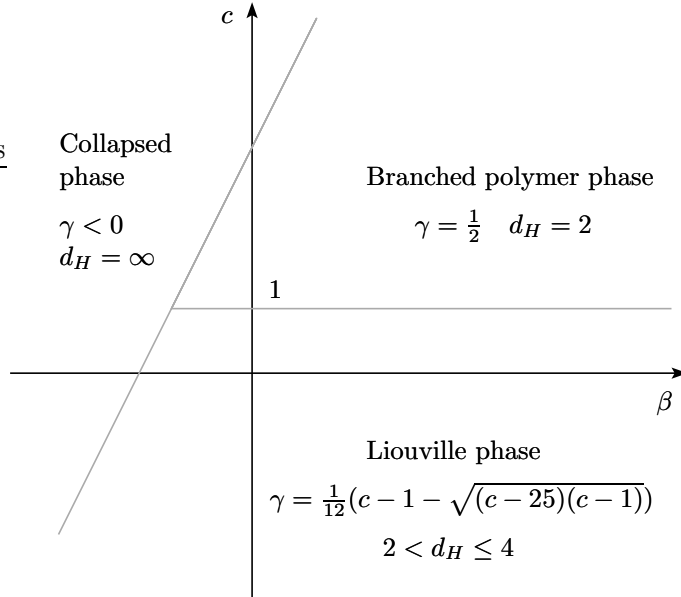


Figure 3.1: Schematic phase structure of two-dimensional simplicial quantum gravity, where the parameters are the central charge of the matter fields c and the measure term exponent β .

To quickly summarize things, we can say that two-dimensional simplicial quantum gravity correctly reproduces the results of the continuum theory, which gives us some hope for the four-dimensional case. We also see that the matter content of the theory can drastically affect its behaviour, both in the discrete case and in the continuum; specifically, if matter fields with a central charge $c > 1$ are included in the theory, it degenerates into an ensemble of branched polymers. Alternatively, we can, through a combination of matter fields and a modified measure, push the system into a third phase where the universe collapses into a compressed, singular disc.

3.1.4 The four-dimensional case

Finally, let us move on to the case that really interests us, namely the four-dimensional one. Here, no analytical results exist, neither for the continuum model nor for its discretized version. However, the discretized partition function has been extensively studied in numerical simulations, and its general properties are by now well-known.

The pure gravity model as defined by (3.13) has two different phases, separated by a critical value κ_2^c of the coupling constant κ_2 . When looked at more closely, both of these phases appear very familiar indeed – they are simply four-dimensional versions of the collapsed and branched polymer phases that we already encountered in two dimensions, with $d_H = 2$, $\gamma = \frac{1}{2}$ in one phase and $d_H \rightarrow \infty$, $\gamma \rightarrow -\infty$ in the

other.⁶ The mechanism that creates these phases is by now well-understood and can be explained in terms of a simple mean-field model [37], which reinforces the view that both of these phases are merely artefacts of the discretization. The problem is that this time, we do not find anything like the Liouville phase, where the model might be expected to reflect continuum physics.

For some time, an alternative possibility was hoped to be found in the phase transition. If this could be shown to be of second or higher order, then the correlation length at the critical point would diverge and one could hope to observe continuum behaviour. Indeed, for a long time the transition was believed to be of second order, and measurements of the Hausdorff dimension near the critical point seemed to indicate a value of $d_H \approx 4$. More detailed studies revealed, however, the existence of a small latent heat, implying that the transition is actually of first order, if weakly so [38, 39].

In other words, we have to conclude that the four-dimensional version of pure simplicial quantum gravity as defined by (3.13) does not have an interesting continuum limit.

3.2 Modifications of the model

If we nevertheless still believe that the idea of simplicial quantum gravity is fundamentally sound – and its success in two dimensions certainly seems to support this view – then we now face the challenge of finding a suitable alteration of the pure gravity model that could improve its critical behaviour. One possibility is that our method of discretizing the model (3.5) is just too naive after all, and that an appropriate modification of the partition function, such as the inclusion of higher order curvature terms [40], might soften the transition to the point where it actually does become of second order. Another, more intriguing idea that we will follow here is that a theory of pure quantum gravity simply might not exist at all, and that the presence of matter of some kind is necessary to formulate a well-defined theory.

3.2.1 Matter fields

As we saw in two dimensions, the matter content of the theory can radically change its behaviour, driving it from the Liouville phase to the branched polymer phase (or vice versa) when passing the $c = 1$ barrier. It therefore seems possible that a similar effect might happen in four dimensions as well, hopefully even creating a four-dimensional analogue to the Liouville phase.

As mentioned in section 3.1.3, the collapse of the two-dimensional model into branched polymers is attributed to the creation of spiky configurations whose free energy can be shown to grow with the logarithm of their length, $F_{spike} \sim (1 - c) \ln \frac{l}{a}$.

⁶The collapsed phase is usually called *crumpled* in the four-dimensional case due to its more complicated geometry. It still has two singular vertices, but they are now connected by a link, which invalidates the ‘collapsed disc’ picture.

It has been suggested [41, 42, 43] that the same kind of mechanism might also be responsible for the occurrence of branched polymers in the four-dimensional case.

Strictly speaking, the conformal gauge cannot be used in four dimensions since we now have more than one free parameter. However, we can at least consider it as a first approximation, assuming that the ‘transverse’ components of the metric enter the calculation only as a correction. Then the free energy of a spike can be calculated as

$$F_{spike} \sim \left(\frac{n_S + \frac{11}{2}n_F + 62n_V - 28}{360} + Q_{grav}^2 - 4 \right) \ln \frac{l}{a} \quad (3.24)$$

where n_S , n_F , and n_V are the numbers of scalar, fermion, and vector fields, respectively, and $Q_{grav}^2 \approx 3.9$ is an estimate of the transverse gravitons’ contribution based on a one-loop calculation. Again we see that, as long as the prefactor is negative, spikes will dominate since we can make l arbitrarily large. Contrary to the two-dimensional case, however, it now looks as if we should *add* matter fields to make the theory more stable, due to the different sign in the free energy. Also contrary to what we saw before, the prefactor is negative in the pure gravity case, *i.e.* for $n_S = n_F = n_V = 0$. This seems to suggest that pure gravity might indeed be ill-defined in four dimensions, and that we should add matter fields to the partition function to obtain a sensible model.

From the prefactors of n_S , n_F , and n_V in (3.24), it seems clear that the various types of matter fields should have very different effects on the model. In particular, scalar fields should produce almost no change unless added in very large numbers; this agrees with earlier observations from numerical simulations [44]. On the other hand, we should expect a strong reaction of the model to the addition of vector fields, which have the largest prefactor.

What we will try, then, is to change the model by adding a variable number of $U(1)$ gauge fields (or actually their non-compact counterparts). The corresponding discrete action was deduced in [45, 46]; on dynamical triangulations it simplifies to

$$S_M = \sum_{\langle ijk \rangle} o_{ijk} \left(A_{ij}^\mu + A_{jk}^\mu + A_{ki}^\mu \right)^2 \quad (3.25)$$

where $\mu = 1, \dots, n_V$. The fields are defined on the links of the triangulation; since these are oriented, we have $A_{ij}^\mu = -A_{ji}^\mu$.

The canonical partition function is now

$$Z(n_4, \kappa_2) = \sum_T \frac{1}{C(T)} \int \prod'_{\langle ij \rangle} dA_{ij} e^{-\kappa_4 n_4 + \kappa_2 n_2 - \sum_{\langle ijk \rangle} o_{ijk} (A_{ij}^\mu + A_{jk}^\mu + A_{ki}^\mu)^2} \quad (3.26)$$

Here, the prime on the product over links indicates that the model now has a number of zero modes coming from the fact that we can simultaneously shift all fields around a given vertex $\langle i \rangle$ by a constant, $A_{ij}^\mu \rightarrow A_{ij}^\mu + \epsilon$, without changing the action. We can deal with these zero modes by considering only a maximal tree for each triangulation (which corresponds to skipping the integration over n_0 field variables).

3.2.2 Measure terms

In (3.26), the integration over matter fields is taken over the link variables, *i. e.* the individual fields themselves. But as can be seen from the action, the physical quantities are actually not these but the plaquette values $A_{ij}^\mu + A_{jk}^\mu + A_{ki}^\mu$. If we assume that the individual fields are only weakly correlated to each other, then we can as a first approximation regard the plaquettes as independent, and simply replace the integration over fields by an integration over plaquette values. We could then immediately perform the matter integrals to get

$$Z(n_4, \kappa_2) = \sum_T \frac{1}{C(T)} \prod_{\langle ijk \rangle} o_{ijk}^\beta e^{-\kappa_4 n_4 + \kappa_2 n_2} \quad (3.27)$$

where $\beta \sim -n_V/2$. This partition function, *if* it should turn out to be essentially equivalent to (3.26), would have a number of practical advantages for numerical simulations; for one thing, they should be easier and quicker to perform, since no field updates have to be made, for another, we can choose non-integer values of β , which is obviously not possible in the case of n_V .

3.3 The strong coupling expansion

In the original work that this chapter is based on [47, 48], the partition functions (3.26) and (3.27) were studied using two different methods, namely numerical simulations as described in chapter 2 and a non-statistical method known as the strong coupling expansion. Since this latter method is used here for the first time in the context of four-dimensional simplicial gravity, I will describe it in some detail. It relies on calculating exactly the contributions of some of the smallest configurations to the partition function and extracting from these an estimate of the desired observables, using a suitable method to reduce the inevitable finite size effects as much as possible. Obviously, this scheme can work only if the first few terms of the partition function are really the important ones – we cannot expect it to produce meaningful results if the coupling is too weak, *i. e.* in the crumpled phase. Fortunately, the most interesting developments will be seen to take place in the branched polymer phase, where the strong coupling expansion provides very good results.

3.3.1 Calculation of the series terms

The first thing we need to calculate the series is some reliable method of constructing all distinct triangulations for a given volume. In two dimensions this can be done simply by using the Feynman rules on the equivalent matrix model, but the same is not possible in four dimensions.

Instead, we can exploit the properties of the (p, q) moves, which we know to (a) be ergodic and (b) change the number of 4-simplices by always the same amount no matter what configuration they are used on. In other words, each configuration

with a given n_4 must be accessible in one of these ways: using move (1, 5) on a configuration with $n_4 - 4$ simplices; using (2, 4) on a configuration with $n_4 - 2$ simplices; using (3, 3) on some other triangulation of the same size; or using (4, 2) or (5, 1) on a correspondingly larger configuration.

With this in mind, we can formulate the following step-by-step prescription for constructing all triangulations of a given size n_4 , assuming only that all smaller configurations have already been identified:

- Go through all configurations with $n_4 - 4$ simplices, and successively apply move (1, 5) to each of them in all possible ways (which in this case means, to all vertices). Store all resulting triangulations.
- Go through all configurations with $n_4 - 2$ simplices, and successively apply move (2, 4) to each of them in all possible ways. In this case, this means using it on all links. Again, store everything created in this way.
- Now we have a long list of configurations; unfortunately, not all of them are distinct, since any given triangulation can usually be created from smaller ones in more than one way. To eliminate the surplus copies, we need some sort of distinguishing characteristic – an observable that takes a different value for each distinct geometry. There is no *a priori* obvious choice for such a characteristic; in practice, we simply choose one that seems suitably complicated, and change it whenever it turns out to be no longer sufficient. This means, of course, that we need some reliable method of double-checking the results, in order to judge the efficiency of our current choice of characteristic.
- To this end, we now calculate the symmetry factor $C(T)$ in two different ways, one of which is always correct whereas the other depends on whether our distinguishing characteristic has been chosen properly.

First of all, note that the relation between the symmetry factors of two configurations T_1 and T_2 can also be expressed as the relation between the number of different ways we can use the appropriate (p, q) move to transform T_1 into T_2 and the number of ways we can use that move's inverse to transform T_2 back into T_1 :

$$\frac{C(T_1)}{C(T_2)} = \frac{N(T_1 \rightarrow T_2)}{N(T_2 \rightarrow T_1)} \quad (3.28)$$

Thus, we can calculate the symmetry factor of a newly created configuration by counting the number of ways it can be reached from a smaller system, as well as the number of ways of going back. However, this will work only if we have correctly distinguished all distinct triangulations; otherwise, we will in some cases overcount $N(T_1 \rightarrow T_2)$, and the corresponding symmetry factors will come out wrong.

The other method consists of calculating all symmetry factors directly, by counting the number of equivalent re-labelings of vertices for each triangulation.

In practice, this means taking a configuration, re-labeling the vertices in all possible ways, and checking for each permutation whether it leads back to the original labeling. This may seem like a daunting task at first, given that the number of possible permutations grows like $n_0!$; however, we can defuse this problem by noting that only labels of vertices with the same order have to be permuted among themselves, since exchanging the labels of vertices with different orders leads to these labels then occurring more or less often in the re-labeled version than in the original one, which means the two cannot be the same. Except for a very few highly symmetric configurations, this means that in most cases we only face permutations of at most three or four vertex labels among themselves, which is easily done.

Once we have calculated all the symmetry factors in both ways, we can compare them to each other for all configurations. Disagreement for any configuration means that our chosen characteristic failed to distinguish between two or more configurations, which sends us back to the drawing board to come up with a better choice.

- Once we can be sure that we have correctly identified all configurations that can be constructed ‘from below’, we can make the next step by using move $(3, 3)$ on all of them in all possible ways (*i. e.*, on all triangles). As before, we use our distinguishing characteristic to reduce the resulting list to one of only distinct triangulations, and calculate the symmetry factors to make sure that our choice of characteristic is still a good one. We then compare all the ‘new’ configurations to the original list and drop all those that turn out to already have been constructed earlier. If any genuinely new triangulations remain, they are added to the list, and we again use move $(3, 3)$ in all possible ways on these new configurations. The cycle is repeated until no more new configurations turn up.
- Now we face the one fundamental uncertainty about the whole process, namely the possibility of configurations that can only be reached ‘from above’, *i. e.* those to which moves $(5, 1)$, $(4, 2)$, and $(3, 3)$ cannot be applied. In two dimensions, no such ‘irreducible’ configurations exist, but the same has not been proven in four dimensions. In fact, we can never be sure of having found all of them unless we already know all larger configurations, since in theory it is possible that such a triangulation could be reached only by making a long excursion to extremely large n_4 before going back down.

Since we cannot construct these configurations from any we already have, we hunt for them in Monte Carlo simulations, which of course gives us the additional uncertainty of possibly missing some configurations simply due to the randomness of the method. Fortunately, we can estimate the required length of the Monte Carlo runs to pick up all configurations with a reasonable confidence, since we already know more or less how many configurations there are in total – we do not expect to see large numbers of ‘irreducible’ configurations,

and the results prove us correct.

Once all configurations and their symmetry factors have been found, the rest becomes easy; we can calculate terms of the partition function with any number of gauge fields and/or any power of the measure term by running all the configurations through a simple Maple script.

Apart from the consistency check on the distinguishing characteristic as described above, we also performed extensive tests on the program as a whole by constructing all configurations up to $n_4 = 18$ by hand and comparing them to the results of the program.

3.3.2 The ratio method

Once we have calculated a sufficient number of terms in the strong coupling expansion, the next step is to find a way of extracting physical information out of them.

Our primary aim is to show whether matter fields and/or a modified measure can fundamentally alter the model. We are therefore not too interested in the finer details of the geometry, but rather its overall shape. Thus, our most important observables will again be the susceptibility exponent γ and the Hausdorff dimension d_H . The question is how we can measure these in a way that allows us to control the finite size effects.

The prescription we will use here to calculate γ is called the *ratio method*; it has already been successfully used for the same purpose in the simpler case of two dimensions [49, 50]. To describe it, I will assume that the finite size corrections are of order $o(n_4^{-1})$. Then the partition function is expected to behave as

$$Z(n_4, \kappa_2) \sim e^{\kappa_4^c(\kappa_2)n_4} n_4^{\gamma-3} (1 + o(n_4^{-1})) \quad (3.29)$$

We will have to find an estimate of $\kappa_4^c(\kappa_2)$ before we can deal with γ . To do so, define

$$C_{n_4}^1(\kappa_2) \equiv \frac{Z(n_4, \kappa_2)}{Z(n_4 - 1, \kappa_2)} \quad (3.30)$$

Inserting (3.29), we find to second order

$$\begin{aligned} C_{n_4}^1 &= e^{\kappa_4^c} \left(\frac{n_4}{n_4 - 1} \right)^{\gamma-3} (1 + o(n_4^{-2})) \\ &= e^{\kappa_4^c} \left(1 + \frac{\gamma-3}{n_4} + o(n_4^{-2}) \right) (1 + o(n_4^{-2})) \\ &= e^{\kappa_4^c} \left(1 + \frac{\gamma-3}{n_4} + o(n_4^{-2}) \right) \end{aligned} \quad (3.31)$$

i. e. $C_{n_4}^1$ gives us an estimate of κ_4^c that is correct to order $o(n_4^{-1})$. Next, define

$$C_{n_4}^{p+1} \equiv \frac{1}{p} \left(n_4 C_{n_4}^p - (n_4 - p) C_{n_4-1}^p \right) \quad (3.32)$$

Assuming that $C_{n_4}^p = e^{\kappa_4^c}(1 + o(n_4^p)) = e^{\kappa_4^c}(1 + c_p/n_4^p + d_p/n_4^{p+1} + \dots)$ has already been shown, we see

$$\begin{aligned}
C_{n_4}^{p+1} &= \frac{1}{p} \left(n_4 e^{\kappa_4^c} \left(1 + \frac{c_p}{n_4^p} + \frac{d_p}{n_4^{p+1}} \right) - (n_4 - p) e^{\kappa_4^c} \left(1 + \frac{c_p}{(n_4 - 1)^p} + \frac{d_p}{(n_4 - 1)^{p+1}} \right) \right) \\
&= e^{\kappa_4^c} \left(1 + \frac{c_p}{pn_4^{p-1}} + \frac{d_p}{pn_4^p} - \frac{(n_4 - p)c_p}{p(n_4^p - pn_4^{p-1} + \dots)} - \frac{(n_4 - p)d_p}{p(n_4^{p+1} - (p+1)n_4^p + \dots)} \right) \\
&= e^{\kappa_4^c} \left(1 + \frac{d_p}{pn_4^p} \left(1 - \frac{n_4 - p}{n_4 - p - 1} \right) + o(n_4^{-(p+1)}) \right) \\
&= e^{\kappa_4^c} \left(1 + o(n_4^{-(p+1)}) \right) \tag{3.33}
\end{aligned}$$

so the series $C_{n_4}^p$ gives us better and better estimates of κ_4^c .

Similarly, we can now find an estimate of γ by defining

$$D_{n_4}^1 \equiv n_4 (C_{n_4}^1 - C_{n_4}^2) \tag{3.34}$$

for which, inserting the expressions for $C_{n_4}^1$ and $C_{n_4}^2$ from above, we find

$$\begin{aligned}
D_{n_4}^1 &= n_4 \left((1 - n_4) C_{n_4}^1 + (n_4 - 1) C_{n_4-1}^1 \right) \\
&= n_4 \left((1 - n_4) e^{\kappa_4^c} \left(1 + \frac{\gamma - 3}{n_4} + \frac{d_1}{n_4^2} \right) + (n_4 - 1) e^{\kappa_4^c} \left(1 + \frac{\gamma - 3}{n_4 - 1} + \frac{d_1}{(n_4 - 1)^2} \right) \right) \\
&= e^{\kappa_4^c} (\gamma - 3) \left(1 + \frac{(1 - n_4)d_1}{n_4} + \frac{n_4 d_1}{n_4 - 1} \right) \\
&= e^{\kappa_4^c} (\gamma - 3) \left(1 + o(n_4^{-1}) \right) \tag{3.35}
\end{aligned}$$

Defining the higher order terms as before,

$$D_{n_4}^{p+1} \equiv \frac{1}{p} \left(n_4 D_{n_4}^p - (n_4 - p) D_{n_4-1}^p \right) \tag{3.36}$$

we can again show that each term $D_{n_4}^p$ gives us an estimate of $e^{\kappa_4^c}(\gamma - 3)$ that is correct up to order $o(n_4^{-p})$. Finally, we can estimate γ itself through

$$\frac{D_{n_4}^p}{C_{n_4}^p} + 3 = \gamma \left(1 + o(n_4^{-p}) \right) \tag{3.37}$$

As it turns out, calculation of the Hausdorff dimension d_H from the strong coupling expansion is far more difficult than extracting the susceptibility exponent; here we find that the Monte Carlo simulations actually lead to much better results.

3.3.3 Results

The calculation of the series terms is limited by several factors as n_4 is increased, among them the growing demands of *CPU* time and storage space and the ever

n_4	n_2	$N(n_4, n_2)$	$Z(n_4, n_2)$	n_4	n_2	$N(n_4, n_2)$	$Z(n_4, n_2)$
6	20	1	1	30	74	139	73860
10	30	1	3		76	1276	672821
12	34	1	5		78	1208	564000
14	40	1	15		80	143	46376
16	44	2	$63\frac{3}{4}$	32	80	3886	2351430
18	48	3	110		82	5943	3327045
	50	3	95		84	1700	$817306\frac{7}{8}$
20	52	2	225	34	84	11442	7502430
	54	7	693		86	26337	16396680
22	58	15	2460		88	13231	7545780
	60	7	690		90	922	411255
24	62	34	$8182\frac{1}{2}$	36	88	27765	18929925
	64	34	$7312\frac{1}{2}$		90	112097	74395157
26	66	50	17865		92	85734	54240610
	68	124	39645		94	15298	$8742976\frac{2}{3}$
	70	30	5481	38	92	71295	50097510
28	70	89	$41650\frac{5}{7}$		94	458083	315706725
	72	415	182820		96	490598	328515075
	74	217	$77057\frac{1}{7}$		98	153773	97507410
					100	6848	3781635

Table 3.1: The numbers of existing triangulations $N(n_4, n_2)$ and their pure gravity weights $Z(n_4, n_2)$ for $n_4 = 6, \dots, 38$. The weights have been normalized so that $Z(6, 20) \equiv 1$.

larger difficulties in finding a distinguishing characteristic that still works on all configurations. Despite this, we managed to push the calculation up to $n_4 = 38$ and about 10^6 configurations. The numbers $N(n_4, n_2)$ and weights $Z(n_4, n_2)$ of all configurations created in this way are collected in table 3.1.

When trying to use the ratio method on these weights to extract γ , we find a noticeable oscillation with growing n_4 . In fact, we can clearly distinguish between two separate series, one that is made up from all configurations with $n_4 = 4k$ and one that contains all those with $n_4 = 4k + 2$; both series seem to converge toward the same value, except that one is coming from above and the other from below. The reason for this can be traced back to asymmetric jumps in the maximal integrated curvature when n_4 is increased [51]. Namely, on dynamical triangulations we have a general constraint on the number of triangles, $n_2 \leq 2.5n_4 + 5$ [52], and we also know that the number of triangles must be even. This gives us an actual maximum number of triangles $n_{2,max} = 2.5n_4 + 5$ in the $n_4 = 4k + 2$ series, but only $n_{2,max} = 2.5n_4 + 4$ in the $4k$ series. From (3.9), we see that this means the maximal integrated curvature jumps by $6c_4 - 6$ when going from a $4k$ series term to the next higher $4k + 2$ series term, but only by $4c_4 - 6$ when going from a $4k + 2$ term to the next higher $4k$ term. But as we will see, the system in the large κ_2 phase is always close to the maximal integrated curvature; hence the oscillations. As it turns out that the finite size effects are much less pronounced for the $4k + 2$ series, we restrict ourselves to using these terms.

Effects of the matter fields

The results for γ as a function of κ_2 with a varying number of vector fields are presented in figure 3.2. For pure gravity and large values of κ_2 , we see the susceptibility exponent approaching the branched polymer value $\gamma = \frac{1}{2}$, as expected. For smaller values of the coupling constant, the estimate becomes unstable and meaningless, which is not surprising given the limitations of what is called, after all, the strong coupling expansion. (Below the transition, *i.e.* in the crumpled phase, γ is not defined in any case.)

Adding a single vector field does not seem to have much of an effect on the model, at least in the region where we can trust the strong coupling expansion. But starting with three vector fields, we see a remarkable change in the string susceptibility exponent as it moves away from the branched polymer value and becomes negative. This mirrors the behaviour of two-dimensional simplicial gravity, where the susceptibility exponent goes from $\frac{1}{2}$ to negative values as the system crosses the $c = 1$ barrier and moves into the Liouville phase. It would seem, then, that there exists a related third phase – which we will call *crinkled phase* – in the four-dimensional model also, but only if we add a sufficient number of vector fields. This, of course, is just what we hoped and expected to find.

The existence of the crinkled phase is supported by results of the Monte Carlo simulations, where the system also exhibits a negative susceptibility exponent once the number of vector fields grows beyond 2, with the measured value of γ compatible

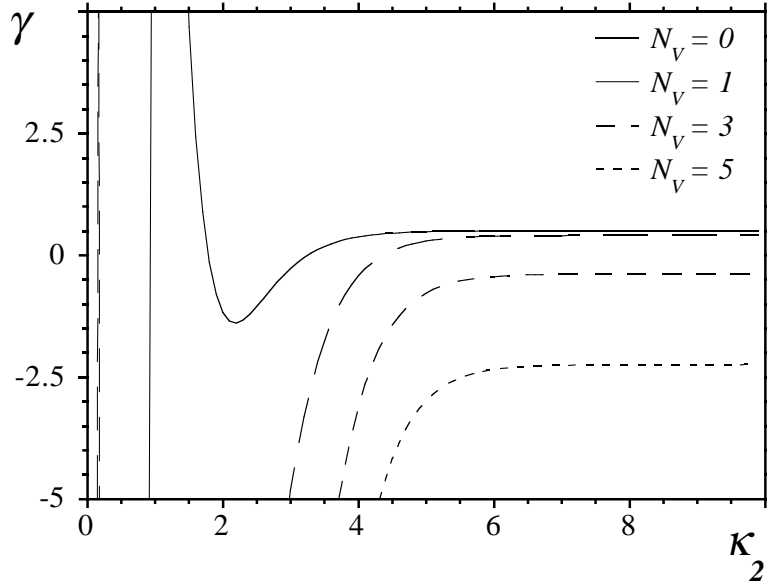


Figure 3.2: The string susceptibility exponent γ , estimated from the strong coupling expansion, as a function of κ_2 for various numbers of vector fields.

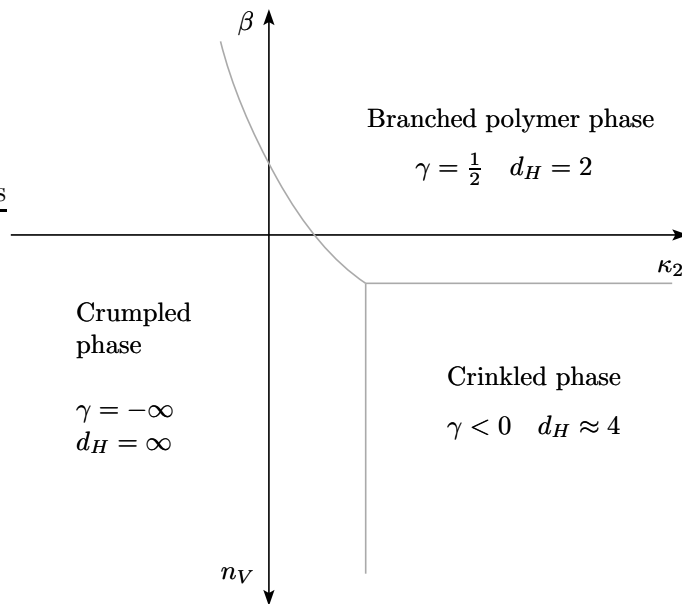


Figure 3.3: Schematic phase structure of four-dimensional simplicial quantum gravity with either n_V gauge fields or a modified measure exponent β .

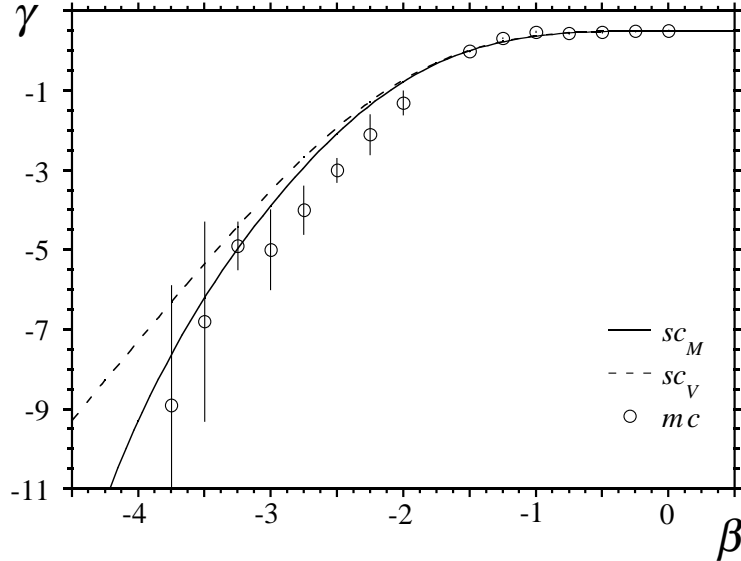


Figure 3.4: The string susceptibility exponent γ as a function of β for $\kappa_2 = 10$ (solid line). For comparison, γ as a function of n_V is also shown, where the identification $\beta \equiv -\frac{n_V}{2} - \frac{1}{4}$ is made on the x axis (dashed line). Finally, results for γ as a function of β from Monte Carlo simulations at $\kappa_2 = 3$ are also included (circles).

with the results of the strong coupling expansion – for example, for $n_V = 3$ and $\kappa_2 = 4.5$ we find in the largest systems we simulated ($n_4 = 16000$) a susceptibility exponent $\gamma = -0.30(6)$, to be compared with a value $\gamma = -0.38$ extracted from the strong coupling series (although at a larger value of κ_2 , since the series is not yet reliable at $\kappa_2 = 4.5$). The Monte Carlo simulations also show a related change in the Hausdorff dimension, which goes from the branched polymer value $d_H = 2$ for pure gravity to $d_H = 3.97(15)$ for $n_V = 3$ and $\kappa_2 = 4.5$ – exactly what one would be hoping to see in a theory of four-dimensional gravity.

Effects of the measure term

We can use the strong coupling expansion with equal ease on the model with a modified measure, calculating the string susceptibility exponent for a varying (negative) exponent β . Figure 3.4 shows the results for $\kappa_2 = 10$. For small absolute β , the modification of the measure has essentially no effect, and the susceptibility exponent retains its branched polymer value of $\gamma = \frac{1}{2}$. Once we decrease β below a certain point, however, γ starts to drop and soon becomes negative, exactly as before.

We can even show the relation between β and n_V by superimposing on the figure a plot of γ from the model with matter fields, setting $\beta = -\frac{n_V}{2} - \frac{1}{4}$ on the x axis; we see that up to about $n_V = 5$, the two curves lie practically on top of each other. Overall, the conclusion seems to be that both matter fields and the kind of modified

measure described here lead to the same kind of effective action, which in turn changes the behaviour of the model by replacing the branched polymer phase with the crinkled phase.

The nature of the crinkled phase

Although the crinkled phase has many similarities to the Liouville phase, on closer inspection it also reveals some worrying features that do not appear in the lower-dimensional case. For one thing, the total curvature in the crinkled phase is very near to its upper bound, which is given by the fact that $n_0 \leq \frac{1}{4}n_4$. But this bound is just a technicality of the discretization, created by the fact that we are using triangulations to regularize space-time; it does not exist in the continuum theory. This might lead us to question our results for the Hausdorff dimension and the susceptibility exponent, since they might have been influenced by the artificial cut-off of the upper bound. Another point is that the largest vertex order – which in the crumpled phase grows linearly with the volume and thus causes that phase’s problems – grows considerably faster in the crinkled phase than in the Liouville phase, although it does remain sub-linear. Finally, the transition point κ_2^c from crumpled to crinkled phase changes with n_4 in a way that makes it difficult to decide whether it will converge in the large n_4 limit; if it does not, the crinkled phase will disappear in the continuum.

On the other hand, we found that just as with the branched polymer phase, the total curvature, while close to the upper bound, does not stick to it; instead, the distribution develops a peak at some point below this bound and then starts to decrease again. From this point of view, the influence of the bound on the measurements of d_H and γ should be small. The largest vertex order, while indeed growing faster than logarithmically as happens in the Liouville phase, does remain sub-linear and thus will become unimportant in the large n_4 limit; one might argue that the details of its growth do not matter as long as it is ensured that no singular points will remain in the continuum. And finally, while it is possible that κ_2^c might move to infinity with $n_4 \rightarrow \infty$, it is just as possible that it might converge to a finite value; for the moment, the numerical data simply does not allow for a definite prediction one way or the other.

There also exists a mean-field argument based on the ‘balls in boxes’ concept [53, 54, 55] that seems to support the view of the crinkled phase being artificial, since it correctly describes many general features of both the crinkled and the branched polymer phase based solely on the existence of the upper bound on the curvature. On the other hand, it also makes some predictions that do not agree with what is observed in the Monte Carlo simulations, such as a first order transition from crumpled to crinkled phase and a latent heat that grows with n_V , whereas the simulations show a transition of third or even higher order and a latent heat that decreases with n_V . These might be taken as just minor failings of an otherwise valid approximation, or as a sign that we should look for something more than a mean-field argument to explain the crinkled phase.

The final conclusion must be that the nature of the crinkled phase is for now

uncertain, and requires further studies before one could make a more definite statement. In particular, one should attempt to push the simulations to larger values of n_4 so as to decide what happens to the transition point.

3.4 Discussion

In the pursuit of this project, we followed two different goals: the study of a modified model of four-dimensional simplicial quantum gravity, in the hope that these modifications might improve the model's critical behaviour; and a test of the applicability of the strong coupling expansion to such a four-dimensional model.

With respect to the modified model, we find that the addition of an appropriate number of matter gauge fields does indeed cause a major change in the behaviour of the model. Essentially, the branched polymer phase of the pure gravity model vanishes and is replaced by a new 'crinkled phase'. The extended tree structure of branched polymers is no longer present in this phase, nor does it have the singular vertices of the crumpled phase; instead, it exhibits a number of similarities to the Liouville phase of two dimensions, such as a negative string susceptibility exponent and a Hausdorff dimension whose measured value is compatible with 4. Also, the transition to the crumpled phase is no longer discontinuous but at least of third order, or even a crossover. This was further confirmed in [56].

We also found that essentially the same effects can be generated by the inclusion of an additional measure factor $\prod o^\beta$ in the partition function. This seems to confirm the assumption that the correlations between the field variables are weak. Further evidence for this was given in [57], where it was shown that the measure factor appears naturally when transforming a model of gauge fields living on the dual links of the lattice to the version of the model we examined here. For the model with fields on the dual links, without the additional factor o_{ijk} in the action, the observed effects of the fields on the geometry are weak.

Despite its similarities to the Liouville phase, the crinkled phase also exhibits a few less appealing features that are not present in the two-dimensional case, such as an integrated curvature that is close to the upper kinematic bound. Also, we cannot yet exclude the possibility that the transition point between crumpled and crinkled phase might move to infinity with growing n_4 . For a decisive answer, we should take the simulations to much larger systems. It might well turn out that vector fields alone are not sufficient to make the model well-defined; if so, an intriguing thought is that it might take an exactly balanced mixture of scalar, vector, and fermion fields to create a physical universe. In any case, we can say that we have shown, contrary to earlier investigations, that the inclusion of matter fields can have a drastic influence on four-dimensional simplicial gravity, making further studies in this direction worthwhile.

In the matter of applying the strong coupling expansion to a four-dimensional triangulated model, we can claim a clear success. We have found a reliable method of calculating successive terms of the series expansion that, apart from one final uncer-

tainty in the form of ‘irreducible’ configurations that cannot be directly constructed from smaller surfaces, does not depend on statistical methods. Calculation of the terms has been taken to $n_4 = 38$, and could conceivably be taken even farther. Problems of increasing *CPU* time and storage space should even now present much less of a difficulty than they were three years ago, when this project was undertaken. The task of finding an ever-more-sensitive distinguishing characteristic could be avoided by a slight modification of the algorithm; rather than demanding that our choice of characteristic be capable of separating every single distinct triangulation, we could use it as only a rough instrument for classifying configurations, and then directly compare all configurations within each category so as to weed out the redundancies.

One practical problem that remains in the application of this method is finding a way of calculating observables while systematically reducing finite size effects. As we saw, the ratio method used here has only a limited range of observables that it can work on; one should certainly try to find other methods that could allow us to access other quantities, such as the Hausdorff dimension, as well.

Chapter 4

One-dimensional structures in models with an area action

Quantized superstring theory is nowadays believed by many to constitute the best bet for a description of quantum gravity. Differently from other attempts, it seems to be not just renormalizable but even finite to each order of its perturbative expansion, and it contains a spin-2 particle that can be interpreted as a graviton in a natural way. Nevertheless, it suffers from the fact that it contains a path integral over surfaces that in general cannot be solved. The only exceptions are the cases $d \leq 1$, where we actually have a prescription for how to perform the integration [58, 59]; and the critical case $d = 10$, where the surface integral decouples completely from the rest of the theory and can therefore be dropped [60]. The generic solution at this point is to accept the ten-dimensional theory as correct and argue that some of these dimensions are ‘compactified’ in our physical universe, making it appear four-dimensional at large enough distances. So far, however, there exists no rigorous prescription for how to perform this compactification.

A different problem comes from the fact that even though all individual terms in the perturbative expansion appear to be finite, the series as a whole is still divergent. In other words, there exists as yet no non-perturbative definition of string theory. A relatively recent proposal to solve this problem comes from the *IKKT model* [61, 62, 63], which provides a sort of quantization prescription where the bosonic and fermionic fields of a supersymmetric string theory are replaced by $n \times n$ Hermitian matrices. This prescription leads to an apparently well-defined partition function that exhibits some striking similarities to the original string theory, and was therefore conjectured to provide an actual constructive definition of same. Consequently, the model was greeted with a lot of enthusiasm, and has since then been investigated in great detail [64, 65, 66, 67, 68, 69].

A much earlier attempt at providing a non-perturbative definition of string theory comes from a discretization of the string world-sheet in terms of dynamical triangulations. In its original formulation, however, this approach turned out to have difficulties. A model of bosonic strings is known to lead to an ill-defined partition

function, due to geometrical defects called spikes [10]. Attempts to discretize a model with space-time supersymmetry [70], which was hoped to cure these defects, have mostly failed; this model also has a local world-sheet symmetry, called κ symmetry, that is explicitly broken on a triangulated lattice, and it is not known how to ensure that it becomes restored in the continuum limit [71]. At this point, research on this approach was more or less abandoned – until the development of the *IKKT* model led, as a sort of by-product, to a new formulation of the supersymmetric model in which the κ symmetry had been gauged away. Thus, a discretization of quantum string theory once more appeared possible as well [72].

In this chapter, we will study some characteristics of both proposals, although the main focus will be on the triangulated model, and the question whether a supersymmetric model with an area action can avoid the singularities encountered in the purely bosonic case. Once we know what is going on in the surface model, we will try to apply our findings to the *IKKT* model – or rather its lower-dimensional counterpart – as well.

4.1 The surface model

Our starting point is the Green-Schwarz *IIB* superstring in the Nambu-Goto form, which is re-written to (a) gauge fix the local κ symmetry and (b) switch the integration to one over internal metrics, which then allows us to do a discretization in terms of dynamical triangulations. The complete calculation can be found in [61]; here I will just sketch the major steps.

The action is

$$S_{IIB} = \int d^2\sigma \left(\sqrt{-\frac{\Sigma^2}{2}} + i \sum_{j=1}^2 \epsilon^{\alpha\beta} \partial_\alpha X^\mu \bar{\theta}^j \Gamma_\mu \partial_\beta \theta^j + \epsilon^{\alpha\beta} \bar{\theta}^1 \Gamma^\mu \partial_\alpha \theta^1 \bar{\theta}^2 \Gamma_\mu \partial_\beta \theta^2 \right) \quad (4.1)$$

where X^μ , $\mu = 1, \dots, 10$, are the bosonic fields; θ_a^1, θ_a^2 , $a = 1, \dots, 16$, are the fermions; (σ_1, σ_2) is a parametrization of the world-sheet; and Σ is defined as

$$\Sigma^{\mu\nu} \equiv \epsilon^{\alpha\beta} (\partial_\alpha X^\mu - i\bar{\theta}^1 \Gamma^\mu \partial_\alpha \theta^1 + i\bar{\theta}^2 \Gamma^\mu \partial_\alpha \theta^2) (\partial_\beta X^\nu - i\bar{\theta}^1 \Gamma^\nu \partial_\beta \theta^1 + i\bar{\theta}^2 \Gamma^\nu \partial_\beta \theta^2) \quad (4.2)$$

Note that this differs from the usual formulation of the model [73] in that one of the fermionic fields has been replaced by an analytic continuation, $\theta_a^2 \rightarrow i\theta_a^2$. The action has two symmetries, the $\mathcal{N} = 2$ space-time supersymmetry

$$\delta_S \theta^1 = \epsilon^1 \quad \delta_S \theta^2 = \epsilon^2 \quad \delta_S X^\mu = i\bar{\epsilon}^1 \Gamma^\mu \theta^1 - i\bar{\epsilon}^2 \Gamma^\mu \theta^2 \quad (4.3)$$

and the κ symmetry

$$\delta_\kappa \theta^1 = \alpha^1 \quad \delta_\kappa \theta^2 = \alpha^2 \quad \delta_\kappa X^\mu = i\bar{\theta}^1 \Gamma^\mu \alpha^1 - i\bar{\theta}^2 \Gamma^\mu \alpha^2 \quad (4.4)$$

where

$$\alpha^1 \equiv \left(1 + \frac{\Sigma^{\mu\nu} [\Gamma_\mu, \Gamma_\nu]}{4\sqrt{-\frac{\Sigma^2}{2}}} \right) \kappa_1 \quad \alpha^2 \equiv \left(1 - \frac{\Sigma^{\mu\nu} [\Gamma_\mu, \Gamma_\nu]}{4\sqrt{-\frac{\Sigma^2}{2}}} \right) \kappa_2 \quad (4.5)$$

The κ symmetry can be gauge fixed by setting $\theta^1 = \theta^2 = \Psi$, which simplifies the action to

$$S'_{IB}(X, \bar{\Psi}, \Psi) = \int d^2\sigma \left(\sqrt{-\frac{\sigma^2}{2}} + 2i\epsilon^{\alpha\beta} \partial_\alpha X^\mu \bar{\Psi} \Gamma_\mu \partial_\beta \Psi \right) \quad (4.6)$$

where

$$\sigma^{\mu\nu} \equiv \epsilon^{\alpha\beta} \partial_\alpha X^\mu \partial_\beta X^\nu \quad (4.7)$$

This action still has the $\mathcal{N} = 2$ supersymmetry, but the transformation laws have to be adjusted to preserve the gauge condition. They can now be written as

$$\begin{aligned} \delta_S^{(1)} \Psi &= -\frac{\sigma^{\mu\nu} [\Gamma_\mu, \Gamma_\nu] \epsilon}{2\sqrt{-\frac{\sigma^2}{2}}} & \delta_S^{(2)} \Psi &= \xi \\ \delta_S^{(1)} X^\mu &= 4i\bar{\epsilon} \Gamma^\mu \Psi & \delta_S^{(2)} X^\mu &= 0 \end{aligned} \quad (4.8)$$

As shown by Schild [74], we can write down an action that is at least classically equivalent to (4.6) if we replace the integration over surfaces expressed in the external coordinates by an integration over internal metrics:

$$S''_{IB}(X, \bar{\Psi}, \Psi) = \int d^2\sigma \sqrt{|g|} \left(\frac{1}{4} \{X^\mu, X^\nu\}^2 - \frac{i}{2} \bar{\Psi} \Gamma_\mu \{X^\mu, \Psi\} \right) \quad (4.9)$$

where $|g|$ is the determinant of the world-sheet metric, and the Poisson bracket is defined as

$$\{X, Y\} \equiv \frac{1}{\sqrt{|g|}} \epsilon^{\alpha\beta} \partial_\alpha X \partial_\beta Y \quad (4.10)$$

The supersymmetry now becomes

$$\begin{aligned} \delta_S^{(1)} \Psi &= -\frac{1}{2} \{X^\mu, X^\nu\} [\Gamma_\mu, \Gamma_\nu] \epsilon & \delta_S^{(2)} \Psi &= \xi \\ \delta_S^{(1)} X^\mu &= i\bar{\epsilon} \Gamma^\mu \Psi & \delta_S^{(2)} X^\mu &= 0 \end{aligned} \quad (4.11)$$

At least formally, then, we can write down a quantum theory of the IB superstring as a path integral over this action,

$$Z = \int \mathcal{D}g_{\mu\nu} \mathcal{D}X \mathcal{D}\bar{\Psi} \mathcal{D}\Psi e^{-S''_{IB}(X, \bar{\Psi}, \Psi)} \quad (4.12)$$

It should be noted that while, as mentioned above, the string theory is defined only in $d = 10$ dimensions, we can in general formulate the integral as a supersymmetric surface model in $d = 3, 4, 6,$ and 10 dimensions. As we will see, many important properties, especially the long distance behaviour, turn out to be essentially the same in any dimension.

4.1.1 Discretization of the surface model

We now want to discretize the integral (4.12) in terms of dynamical triangulations, following essentially the suggestions in [72].

For simplicity, I will fix the number of dimensions from the start to be $d = 4$, since that is where the numerical simulations will be performed. Generalization of our arguments to higher dimensions is straightforward, and will be addressed once we understand what happens in four dimensions.

The choice of $d = 4$ also determines the fermionic variables to be either Majorana or Weyl spinors, at least if we want to have supersymmetry. Either choice will lead to the same results [67]; we will here take them to be Weyl spinors. We also choose to put both the bosonic and the fermionic fields on the vertices of the lattice.

With these choices, we can write down the canonical partition function for the triangulated model as

$$Z(n_2) = \sum_T \frac{1}{C(T)} \int \prod_{i=1}^{n_0} d^4 X_i \prod_{i=1}^{n_0} d^4 \bar{\Psi}_i d^4 \Psi_i e^{-S_B(X_i) - S_F(X_i, \bar{\Psi}_i, \Psi_i)} \quad (4.13)$$

Here, the products of integration variables have primes attached to them because, as we will see, there are zero modes that have to be removed to get a well-defined partition function. Note that since we are studying triangulations with an internal dimension of 2, the numbers of triangles and vertices are dependent on each other; choosing a specific value of n_2 automatically fixes n_0 (see section 3.1.3 for details).

The action of the discrete model

To write down the discretized action $S = S_B + S_F$, we first need a discrete version of the Poisson bracket $\{X, Y\}$. In [72], this is defined as an average value for each triangle,

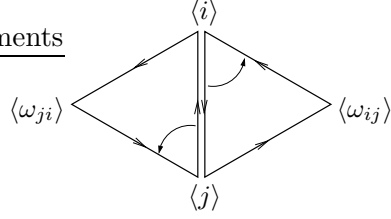
$$\{X, Y\}_{ijk} \equiv \frac{1}{2A} \epsilon^{ijk} (X_{jk} Y_{ki} - Y_{jk} X_{ki}) \quad (4.14)$$

where $X_{ij} \equiv X_i - X_j$ and $A \equiv \frac{\sqrt{3}}{4} a^2$ is the triangle area. Using this, we find

$$S_B(X_i) = \frac{2}{A} \sum_{\langle ij k \rangle} \left\{ - \left((X_{ij}^2)^2 + (X_{jk}^2)^2 + (X_{ki}^2)^2 \right) + 2 \left(X_{ij}^2 X_{jk}^2 + X_{jk}^2 X_{ki}^2 + X_{ki}^2 X_{ij}^2 \right) \right\} \quad (4.15)$$

$$S_F(X_i, \bar{\Psi}_i, \Psi_i) = \frac{i}{12} \sum_{\langle ij \rangle} \bar{\Psi}_i^a \Gamma_{\mu}^{ab} \Psi_j^b \left(X_{\omega_{ij}}^{\mu} - X_{\omega_{ji}}^{\mu} \right) \quad (4.16)$$

Here, $\langle \omega_{ij} \rangle$ and $\langle \omega_{ji} \rangle$ denote the remaining two vertices of the two triangles that contain the link $\langle ij \rangle$. Specifically, $\langle \omega_{ij} \rangle$ is defined to be the neighbouring vertex of $\langle i \rangle$ that comes after $\langle j \rangle$ when going counterclockwise around $\langle i \rangle$:



So far, we have not yet used the fact that $\bar{\Psi}_i, \Psi_i$ are Weyl fermions, *i. e.* that they have a fixed handedness. Mathematically, this means that we can write

$$\Psi_i = \frac{1}{2}(1 + \Gamma_5)\Psi_i \quad \bar{\Psi}_i = \bar{\Psi}_i \frac{1}{2}(1 - \Gamma_5) \quad (4.17)$$

If we choose the following definition of the Dirac matrices (chiral representation):

$$\Gamma_0 = \begin{pmatrix} 0 & -\sigma_0 \\ \sigma_0 & 0 \end{pmatrix} \quad \Gamma_i = \begin{pmatrix} 0 & \sigma_i \\ \sigma_i & 0 \end{pmatrix} \quad \Gamma_5 = \begin{pmatrix} \mathbb{1} & 0 \\ 0 & -\mathbb{1} \end{pmatrix} \quad (4.18)$$

where σ_i are the Pauli matrices and $\sigma_0 \equiv i\mathbb{1}$, then (4.17) becomes

$$\Psi_i = \begin{pmatrix} \mathbb{1} & 0 \\ 0 & 0 \end{pmatrix} \Psi_i \quad \bar{\Psi}_i = \begin{pmatrix} 0 & 0 \\ 0 & \mathbb{1} \end{pmatrix} \bar{\Psi}_i \quad (4.19)$$

which means we can express the fermionic variables in terms of two-component spinors $\bar{\psi}_i, \psi_i$:

$$\bar{\Psi}_i = (0, \bar{\psi}_i) \quad \Psi_i = \begin{pmatrix} \psi_i \\ 0 \end{pmatrix} \quad (4.20)$$

We can therefore re-write the fermionic part of the action as

$$S_F(X_i, \bar{\psi}_i, \psi_i) = i \sum_{\langle ij \rangle} \bar{\psi}_i^a f_{ij}^\mu \sigma_\mu^{ab} \psi_j^b \quad (4.21)$$

where we have also defined

$$f_{ij}^\mu \equiv \frac{1}{12} (X_{\omega_{ij}}^\mu - X_{\omega_{ji}}^\mu) \quad (4.22)$$

Obviously, the f_{ij}^μ are real and antisymmetric in the lattice indices ij . Also, it follows from the definition of $\langle \omega_{ij} \rangle$ that for each vertex $\langle i \rangle$, the sum of f_{ij}^μ over all neighbouring vertices $\langle j \rangle$ vanishes:

$$\sum_{\langle j \rangle : \langle ij \rangle} f_{ij}^\mu = 0 \quad (4.23)$$

Here, the expression ‘ $\langle j \rangle : \langle ij \rangle$ ’ is just a shorthand notation for ‘all vertices $\langle j \rangle$ such that $\langle ij \rangle$ is an existing link on the triangulation’, a convention that I will use throughout the remainder of this chapter.

Zero modes in the action

Now that we know the discretized form of the action, we can see that there are two zero modes that we have to deal with.

One follows from the invariance of S under translations of the bosonic fields, $X_i \rightarrow X_i + \delta$. This is because the coordinates never enter directly into the action but only as differences between vertices $X_i - X_j$, so that any global translation drops right out. We can fix this zero mode by keeping the system's center of mass fixed at some given point, preferably the origin. Technically, this introduces a delta function $\delta^4(\sum X_i)$ in the partition function.

The other zero mode comes from a similar effect in the fermionic sector, namely invariance of the action under a change $\psi_i \rightarrow \psi_i + \epsilon$, $\bar{\psi}_i \rightarrow \bar{\psi}_i + \bar{\epsilon}$. This follows from the properties of the f_{ij}^μ , in particular equation (4.23). Specifically, the change in the action under a translation of the fermions is

$$\begin{aligned}
\delta S_F &= i \sum_{\langle ij \rangle} \bar{\epsilon} f_{ij}^\mu \sigma_\mu \psi_j + i \sum_{\langle ij \rangle} \bar{\psi}_i f_{ij}^\mu \sigma_\mu \epsilon + i \sum_{\langle ij \rangle} \bar{\epsilon} f_{ij}^\mu \sigma_\mu \epsilon \\
&= \frac{i}{2} \sum_{\langle j \rangle} \bar{\epsilon} \sigma_\mu \psi_j \sum_{\langle i \rangle: \langle ij \rangle} f_{ij}^\mu + \frac{i}{2} \sum_{\langle i \rangle} \bar{\psi}_i \sigma_\mu \epsilon \sum_{\langle j \rangle: \langle ij \rangle} f_{ij}^\mu + \frac{i}{2} \bar{\epsilon} \sigma_\mu \epsilon \sum_{\langle i \rangle} \sum_{\langle j \rangle: \langle ij \rangle} f_{ij}^\mu \\
&= 0
\end{aligned} \tag{4.24}$$

We can remove this zero mode by skipping the integration over one pair of fermionic variables in the partition function, for example ψ_{n_0} and $\bar{\psi}_{n_0}$. Technically, this amounts to inserting an additional product $\bar{\psi}_{n_0} \psi_{n_0}$, which for Grassmann variables acts like a delta function.

The fermionic determinant

As the final step, we can integrate out the fermions. This results in a factor $|\mathcal{M}_{ij}^{ab}|$, where

$$\mathcal{M}_{ij}^{ab} \equiv i f_{ij}^\mu \sigma_\mu^{ab} \quad i, j = 1, \dots, n_0 - 1 \quad a, b = 1, 2 \tag{4.25}$$

is the matrix that appears in (4.21), with the two rows and columns that correspond to the vertex $\langle n_0 \rangle$ crossed out because of the fermionic ‘delta function’. Note that despite having four indices this is just a two-dimensional matrix; each combination of indices $\binom{a}{i}$, $\binom{b}{j}$ actually corresponds to only a single matrix index I, J . The size of the matrix can be read off as $2(n_0 - 1) \times 2(n_0 - 1)$.

If we want to perform numerical simulations, it is essential to have a non-negative integrand; otherwise we would encounter the so-called sign problem, which makes any attempt at a numerical treatment all but futile. Fortunately, it is possible to show that in $d = 4$ the determinant $|\mathcal{M}_{ij}^{ab}|$ is in fact non-negative. To see this, take any eigenvalue λ of \mathcal{M}_{ij}^{ab} , together with its corresponding eigenvector l_i^a :

$$\left(i f_{ij}^0 \sigma_0^{ab} + i f_{ij}^1 \sigma_1^{ab} + i f_{ij}^2 \sigma_2^{ab} + i f_{ij}^3 \sigma_3^{ab} \right) l_j^b = \lambda l_i^a \tag{4.26}$$

Now take the complex conjugate of this equation to get

$$\left(i f_{ij}^0 \sigma_0^{ab} - i f_{ij}^1 \sigma_1^{ab} + i f_{ij}^2 \sigma_2^{ab} - i f_{ij}^3 \sigma_3^{ab} \right) (l_j^b)^* = \lambda^* (l_i^a)^* \quad (4.27)$$

because σ_1 and σ_3 are real, whereas σ_0 and σ_2 are purely imaginary. Next, multiply the equation by σ_2 from the left:

$$\left(i f_{ij}^0 \sigma_2^{ca} \sigma_0^{ab} - i f_{ij}^1 \sigma_2^{ca} \sigma_1^{ab} + i f_{ij}^2 \sigma_2^{ca} \sigma_2^{ab} - i f_{ij}^3 \sigma_2^{ca} \sigma_3^{ab} \right) (l_j^b)^* = \lambda^* \sigma_2^{ca} (l_i^a)^* \quad (4.28)$$

Finally, use the fact that σ_2 commutes with σ_0 but anticommutes with σ_1 and σ_3 to get

$$\left(i f_{ij}^0 \sigma_0^{ca} + i f_{ij}^1 \sigma_1^{ca} + i f_{ij}^2 \sigma_2^{ca} + i f_{ij}^3 \sigma_3^{ca} \right) \sigma_2^{ab} (l_j^b)^* = \lambda^* \sigma_2^{ca} (l_i^a)^* \quad (4.29)$$

In other words, if λ is an eigenvalue of \mathcal{M}_{ij}^{ab} , then so is λ^* , to the eigenvector $(\sigma_2^{ca} (l_i^a)^*)$. But since the determinant is just the product of the eigenvalues, and $\lambda \lambda^* = (\text{Re} \lambda)^2 + (\text{Im} \lambda)^2$ is both real and non-negative, we find $|\mathcal{M}_{ij}^{ab}| \geq 0$ for any possible configuration.

Note that all this is true *only* in four dimensions, which is the main reason for our choice of d .

The partition function of the discrete model

We can now write down the final form of the partition function that we want to analyze:

$$Z(n_2, \gamma) = \sum_T \frac{1}{C(T)} \int \prod_{i=1}^{n_0} d^4 X_i^\mu \delta^4 \left(\sum X_i^\mu \right) |\mathcal{M}_{IJ}|^\gamma e^{-S_B(X_i^\mu)} \quad (4.30)$$

Here, we have introduced the additional parameter γ as just a convenient way to distinguish between several cases that we want to look at. Namely, we will be interested in the choices $\gamma = 0, 1, 2$, which correspond to the purely bosonic model, the supersymmetric model, and a model with Dirac fermions instead of Weyl fermions, respectively.

4.2 Spikes and needles

As it turns out, the model as defined above has serious problems both without and with ‘too many’ fermions; in fact, we will show that the partition function (4.30) can be well-defined only in the supersymmetric case $\gamma = 1$. The reason for this can be found in the appearance of so-called ‘flat directions’ in the action – valleys of small and constant values of the action that extend outward to very large and deformed-looking configurations, which can cause the partition function to blow up.

In this particular case, the bosonic action S_B is just the sum of all triangle areas squared. Therefore, if we can find ways of deforming some or all of the triangles into

pathological shapes without affecting their areas, we are heading towards trouble, because we can then expect the partition function to pick up large contributions from these configurations as they are not suppressed by the action.

4.2.1 The bosonic case

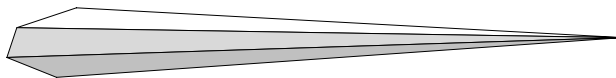
We will start by looking at possible singularities in the purely bosonic model. As we will see, there are two different ways in which the flat directions of the action can affect the partition function.

Spikes

One way of creating deformed triangles has actually been known for a long time, going back to [10]. There, it was shown that for the purely bosonic model these configurations lead to a divergence of the partition function. I will not reproduce the rigorous proof here, but rather try to give a more intuitive argument that will tie in nicely with the arguments presented in the next section.



Choose a vertex $\langle i \rangle$ anywhere on the configuration, and find all its neighbouring triangles. Take all the links that lie opposite to $\langle i \rangle$ on these triangles (*i.e.*, those that form the boundary of $\langle i \rangle$'s neighbourhood), and shrink them to lengths of order $\sim 1/l$, where l is large. Simultaneously, we can now stretch all the links meeting in $\langle i \rangle$ to lengths of order $\sim l$ and still leave all triangles in the neighbourhood of $\langle i \rangle$ with an area of order ~ 1 .¹ Since we can vary l freely, this means we can remove $\langle i \rangle$ arbitrarily far from the rest of the configuration without affecting the action. The result is a *spike*:



Of course, just because it looks strange does not mean that a spike is necessarily a problem. We can examine this point in more detail by trying to estimate a spike's contribution to the partition function. Since the action remains almost fixed during the creation of a spike, all we have to do is look at the entropy factor. We will see that a simple power-counting argument is enough for this purpose.

Assume that we have a spike $\langle i \rangle$ of maximum length l , *i.e.* the coordinates of $\langle i \rangle$ are all of order $\sim l$. Then the entropy factor for the spike itself is $\sim l^4$, since we are in $d = 4$ dimensions. On the other hand, all the vertices on the boundary must be restricted to be within a distance of $\sim 1/l$ from their neighbouring boundary vertices. In other words, we can choose one of them freely, but then all the others

¹Obviously, shrinking the link lengths on the boundary also affects triangle areas outside the neighbourhood of $\langle i \rangle$, but only in a favourable direction, *i.e.* if anything making them smaller.

have positions that are fixed to within $\sim 1/l$. This provides an additional factor $\sim l^{-4(o_i-1)}$. If we now integrate over all but one vertex coordinate, we are left with

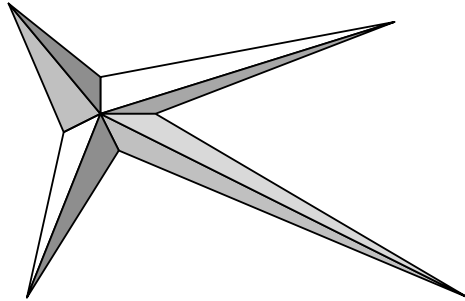
$$Z_{spike} \sim \int dl l^{-4(o_i-2)-1} \quad (4.31)$$

We can interpret the integrand as a probability distribution for the spike length:

$$p(l) \sim l^{-4(o_i-2)-1} \quad (4.32)$$

Since the order of a vertex on a two-dimensional triangulation is always at least 3, this gives us a worst-case distribution of $p(l) \sim l^{-5}$. So the spike's contribution to the partition function is still integrable, and the partition function itself still well-defined. However, because they are suppressed only by a power law, we can expect spikes of arbitrary length to appear in the simulations, and as a result the distribution's higher moments will have no finite expectation values.

Furthermore, the situation can become worse if we consider not just one spike, but several in close proximity to each other. For example, take a configuration as it has been drawn below, with four spikes of order 3 grouped around a central vertex:



In this case, the entropy factor for the spikes is l^{16} , and we have to restrict four vertices to be within a distance of $\sim 1/l$ from the central one, giving rise to another factor l^{-16} . If we again integrate over all but one coordinate, we end up with a distribution

$$p(l) \sim l^{-1} \quad (4.33)$$

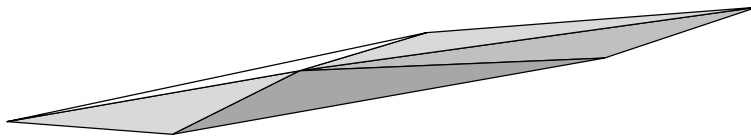
that leads to a logarithmic divergence of the partition function. This is exactly the result of the rigorous proof given in [10].

Needles

In the last section we created a deformed triangle of constant area by shrinking its base while simultaneously increasing its height. We can create another kind of deformation by doing exactly the reverse: lengthening the base of a triangle while decreasing its height. Differently from a spiky triangle with two long links and a short one, this results in a triangle with three long links, as pictured below.



On the surface, it would seem that such a triangle should be even more likely than a spike, because there is no need for restricting the distance between vertices and thus no corresponding entropy ‘penalty’. However, the fact that there is no short link on this kind of triangle implies that, differently from a spike, a deformation like this cannot appear as only a local phenomenon. Namely, an elongated triangle without any short links can only have neighbouring triangles that are all elongated in the same way; otherwise, there would be at least one triangle with a long base and a not-so-small height, resulting in a large area that is exponentially suppressed by the action. Since any two triangles on a simplicial manifold can be connected by a path of neighbouring triangles, it immediately follows that if just one triangle is elongated, then all of them have to be. The result is a configuration that is elongated as a whole – a basically one-dimensional construct that we call a ‘needle’.



We can estimate the likelihood of a needle being created by the same kind of power-counting argument as we used before. Since we now consider the entire configuration, we have to take into account the model’s bosonic zero mode; we can deal with it here by keeping one vertex position fixed. Consequently, this vertex then contributes only a factor of 1. One other vertex can be freely chosen from within a sphere of radius l around the fixed one, thus contributing an entropy factor of $\sim l^4$. Once this vertex has been chosen, the direction of the needle has been determined; the $n_0 - 2$ other vertices will have one ‘free’ coordinate of order $\sim l$ corresponding to this direction, and three coordinates that must be restricted to lie within a distance of $\sim 1/l$ from the needle’s principal axis so that the triangle areas can all remain approximately constant. Thus, we get another factor $\sim l^{-2(n_0-2)}$. Putting them all together and integrating as before, we end up with a distribution

$$p(l) = l^{-2n_0+7} \tag{4.34}$$

Obviously, this means that needles will always be strongly suppressed except on some of the smallest configurations – starting with $n_0 = 7$, even a single spike will be more likely than a needle configuration –, which is, of course, why needles have not been observed so far, spikes causing far greater singularities. Even so, it should be noted that just like spikes, needles are suppressed only by a power law.

4.2.2 The supersymmetric case

Next, we can try to predict what will change in the model if we add fermionic variables to it.

The physical reason behind doing this is the hope that fermionic repulsion should keep the vertices from moving too close to each other, thus preventing the creation of spikes that rely on the possibility of arbitrarily shortening links between vertices. On the other hand, given the arguments above, it might be expected that the presence of fermions could enhance needles, since a needle configuration consists of vertices that are all far removed from each other.

From a more technical point of view, the inclusion of fermions results in an extra factor $|\mathcal{M}_{IJ}|$ that is a product of link lengths. Since spikes and needles are both governed by powers of link lengths, it seems likely that the distributions of both could be substantially altered by the fermionic determinant. We can try to predict the changes by including the determinant in our power-counting arguments. Even at this point, however, it seems already obvious that the results can only be power laws again; we will not see an exponential suppression of either spikes or needles. Nevertheless, we can at least hope for a well-defined partition function.

Spikes in the model with fermions

As can be seen from the definition of \mathcal{M}_{IJ} , it is structured in such a way that with each vertex $\langle i \rangle$ can be associated two rows and two columns that contain only distances between neighbours of $\langle i \rangle$. If $\langle i \rangle$ is a spike of length l , we therefore have two rows and columns with entries that are all of order $\sim 1/l$. Since the diagonal elements of \mathcal{M}_{IJ} are all zero, each non-vanishing term in the sum that constitutes the determinant $|\mathcal{M}_{IJ}|$ must contain exactly four entries from these two rows and columns. Thus, each spike contributes a factor l^{-4} to the fermionic determinant.

At a first glance, we would conclude from this that a single spike should now have a distribution $p(l) \sim l^{-9}$ rather than $\sim l^{-5}$ as before, and that the formerly worse case of having k spikes grouped around a central vertex should have $p(l) \sim l^{-4k-1}$ rather than $\sim l^{-1}$, thus rendering spikes, if not harmless, then at least no longer capable of causing actual divergences of the partition function.

However, this argument is a bit too naive, since the fermionic matrix also contains entries of order $\sim l$ corresponding to links on the boundary of $\langle i \rangle$. Therefore it seems likely that at least in its leading terms the determinant should be more singular than the power $\sim l^{-4k}$ we just claimed. Nevertheless, the end result should still be one of spikes being more strongly suppressed than in the purely bosonic model. We will examine this point further in the numerical part.

Needles in the model with fermions

Since needles are a global phenomenon, we will for an estimate of their link length distribution have to consider the entire determinant and its contribution to the partition function as a whole. More precisely, since we want to see whether the determinant turns needles into a more severe singularity, we need to know the behaviour of the determinant's leading term.

We already know that on a needle configuration every vertex position has one

‘large’ component of order $\sim l$ and three ‘small’ components of order $\sim l^{-1}$. From the definition of \mathcal{M}_{IJ} , it is clear that this means we can find terms of order $\sim l$ in each row and each column of the determinant. At a first glance, it would therefore seem obvious that the leading term should simply be a product of some of these large components, and since \mathcal{M}_{IJ} is a $2(n_0 - 1) \times 2(n_0 - 1)$ matrix, the result should be of order $\sim l^{2(n_0-1)}$. Inserting this into (4.34) would give us

$$p(l) \sim l^{-2n_0+7+2(n_0-1)} = l^5 \quad (4.35)$$

leading to a fatal singularity and an ill-defined partition function.

Fortunately, however, this turns out to be wrong, in that some of the largest terms of $|\mathcal{M}_{IJ}|$ can be shown to cancel out. More precisely, we will see that both the leading and the next-to-leading terms are identically zero, leaving us with a contribution $\sim l^{2(n_0-5)}$ from the determinant and thus a total distribution

$$p(l) \sim l^{-2n_0+7+2(n_0-5)} = l^{-3} \quad (4.36)$$

which is perfectly integrable.

To prove the disappearance of the first two terms of $|\mathcal{M}_{IJ}|$, we will use arguments from perturbation theory. Define a more general matrix

$$\mathcal{M}_{IJ}(\epsilon) \equiv -\mathcal{M}_{IJ}^0 + i\epsilon\mathcal{M}_{IJ}^1 \equiv -\begin{pmatrix} f_{ij}^0 & 0 \\ 0 & f_{ij}^0 \end{pmatrix} + i\epsilon \begin{pmatrix} f_{ij}^3 & f_{ij}^1 + if_{ij}^2 \\ f_{ij}^1 - if_{ij}^2 & -f_{ij}^3 \end{pmatrix} \quad (4.37)$$

For $\epsilon = 1$, this describes a ‘typical’ configuration from the bulk of the distribution, whereas for $\epsilon = 0$, it defines an entirely one-dimensional construct. (Specifically, a construct pointing in the 0-direction; but the direction is irrelevant since the model is rotationally invariant.) An *almost* one-dimensional configuration, then, can be described as a small perturbation around $\mathcal{M}_{IJ}(0)$. We will look successively at the zeroth, first, and second orders of the perturbation expansion. For now, we assume n_0 to be even.

To 0th order, note that f_{ij}^0 has at least one vanishing eigenvalue, since for an entirely one-dimensional configuration $X_i^\mu = (X_i^0, 0, 0, 0)$ the action in (4.30) gains an additional invariance, namely the transformation $\psi_i \rightarrow \psi_i + \alpha X_i^0$, and thus also an additional zero mode.² The corresponding zero eigenvector of f_{ij}^0 is

$$v_i^0 = X_i^0 - X_{n_0}^0 \quad (4.38)$$

Consequently, \mathcal{M}_{IJ}^0 must have at least two zero eigenvectors a_I^0 and b_I^0 , which we can write as

$$a_I^0 = \begin{pmatrix} v_i^0 \\ 0 \end{pmatrix} \quad b_I^0 = \begin{pmatrix} 0 \\ v_i^0 \end{pmatrix} \quad (4.39)$$

²This is a discrete remnant of a much more general invariance $\psi(\xi) \rightarrow \psi(\xi) + \alpha h(X^0(\xi))$ of the continuum action (4.9), where h is an arbitrary function.

Thus, we have $|\mathcal{M}_{IJ}^0| = 0$, and therefore no terms of order ϵ^0 in the determinant of $\mathcal{M}_{IJ}(\epsilon)$.

Now consider a small perturbation $i\epsilon\mathcal{M}_{IJ}^1$, which will change the (twice degenerate) eigenvalues λ_i of \mathcal{M}_{IJ}^0 to $\lambda_i + i\epsilon\Delta_i$ and $\lambda_i - i\epsilon\Delta_i^*$, respectively. In particular, we have a first order correction to the zero eigenvalues of \mathcal{M}_{IJ}^0 that I will call Δ_0 . It obeys the equation

$$\begin{vmatrix} a_I^0\mathcal{M}_{IJ}^1a_J^0 - \Delta_0 & a_I^0\mathcal{M}_{IJ}^1b_J^0 \\ b_I^0\mathcal{M}_{IJ}^1a_J^0 & b_I^0\mathcal{M}_{IJ}^1b_J^0 - \Delta_0 \end{vmatrix} = 0 \quad (4.40)$$

or if we use (4.37) and (4.39) to re-write it in terms of v_i^0 ,

$$\begin{vmatrix} v_i^0 f_{ij}^3 v_j^0 - \Delta_0 & v_i^0 f_{ij}^1 v_j^0 + i v_i^0 f_{ij}^2 v_j^0 \\ v_i^0 f_{ij}^1 v_j^0 - i v_i^0 f_{ij}^2 v_j^0 & -v_i^0 f_{ij}^3 v_j^0 - \Delta_0 \end{vmatrix} = 0 \quad (4.41)$$

But we already know that the f_{ij}^μ are all antisymmetric, which implies $v_i^0 f_{ij}^\mu v_j^0 = 0$ and thus $\Delta_0 = 0$ from the equation above. In other words, both zero eigenvalues remain intact to first order, which means there will be no terms proportional to ϵ^2 either. Therefore, the leading terms of $|\mathcal{M}_{IJ}|$ must be at least of order ϵ^4 . As the numerical simulations show, terms of this order do indeed show up generically.

Accordingly, we can now predict that the determinant will contribute a leading term that consists of $2n_0 - 6$ ‘long’ components and 4 ‘short’ ones, *i. e.* it will be of order $l^{2n_0-6}l^{-4} = l^{2n_0-10}$. Inserting this into our power-counting argument leads to the distribution (4.36).

We still have to deal with the case of odd n_0 , which turns out to lead to a somewhat different result. In this case, f_{ij}^0 is an even by even antisymmetric matrix, which means that it has pairs of eigenvalues λ and $-\lambda$. In particular, this means that it must have an even number of zero eigenvectors. Since we know, by the same arguments as above, that it has at least one of these eigenvectors, it therefore must have at least two, which we call v_i^0 and w_i^0 . Accordingly, we find that \mathcal{M}_{IJ}^0 has not two but four zero eigenvectors, which we write as

$$a_I^0 = \begin{pmatrix} v_i^0 \\ 0 \end{pmatrix} \quad b_I^0 = \begin{pmatrix} w_i^0 \\ 0 \end{pmatrix} \quad c_I^0 = \begin{pmatrix} 0 \\ v_i^0 \end{pmatrix} \quad d_I^0 = \begin{pmatrix} 0 \\ w_i^0 \end{pmatrix} \quad (4.42)$$

This leads to a somewhat more complicated expression for the first order correction Δ_0 , namely

$$\begin{vmatrix} a_I^0\mathcal{M}_{IJ}^1a_J^0 - \Delta_0 & a_I^0\mathcal{M}_{IJ}^1b_J^0 & a_I^0\mathcal{M}_{IJ}^1c_J^0 & a_I^0\mathcal{M}_{IJ}^1d_J^0 \\ b_I^0\mathcal{M}_{IJ}^1a_J^0 & b_I^0\mathcal{M}_{IJ}^1b_J^0 - \Delta_0 & b_I^0\mathcal{M}_{IJ}^1c_J^0 & b_I^0\mathcal{M}_{IJ}^1d_J^0 \\ c_I^0\mathcal{M}_{IJ}^1a_J^0 & c_I^0\mathcal{M}_{IJ}^1b_J^0 & c_I^0\mathcal{M}_{IJ}^1c_J^0 - \Delta_0 & c_I^0\mathcal{M}_{IJ}^1d_J^0 \\ d_I^0\mathcal{M}_{IJ}^1a_J^0 & d_I^0\mathcal{M}_{IJ}^1b_J^0 & d_I^0\mathcal{M}_{IJ}^1c_J^0 & d_I^0\mathcal{M}_{IJ}^1d_J^0 - \Delta_0 \end{vmatrix} = 0 \quad (4.43)$$

which after insertion of (4.37) and (4.42) can be reduced to

$$\left[\Delta_0^2 + \sum_{k=1}^3 \left(v_i^0 f_{ij}^k w_j^0 \right)^2 \right]^2 = 0 \quad (4.44)$$

By definition, the f_{ij}^μ are linear functions of $X_{\omega_{ij}}^\mu$ and $X_{\omega_{ji}}^\mu$, so that we can write $f_{ij}^\mu \equiv f(X_{\omega_{ij}}^\mu, X_{\omega_{ji}}^\mu)$; and the same is true for the eigenvectors, where we have $w_i^\mu \equiv w(X_i^\mu)$. Using this, we find

$$\begin{aligned}
v_i^0 f_{ij}^k w_j^0 &\equiv v(X_i^0) f(X_{\omega_{ij}}^k, X_{\omega_{ji}}^k) w(X_j^0) \\
&= v(X_i^0) f(X_{\omega_{ij}}^k, X_{\omega_{ji}}^k) \left(w(X_j^0) + w(X_j^k) \right) \\
&= v(X_i^0) \left(f(X_{\omega_{ij}}^0, X_{\omega_{ji}}^0) + f(X_{\omega_{ij}}^k, X_{\omega_{ji}}^k) \right) \left(w(X_j^0) + w(X_j^k) \right) \\
&= v(X_i^0) f(X_{\omega_{ij}}^0 + X_{\omega_{ij}}^k, X_{\omega_{ji}}^0 + X_{\omega_{ji}}^k) w(X_j^0 + X_j^k) \\
&= 0
\end{aligned} \tag{4.45}$$

where we first used $f_{ij}^k w_j^k = 0$ to add a term $v(X_i^0) f(X_{\omega_{ij}}^k, X_{\omega_{ji}}^k) w(X_j^k)$; then used $v_i^0 f_{ij}^0 = 0$ to add $v(X_i^0) f(X_{\omega_{ij}}^0, X_{\omega_{ji}}^0) (w(X_j^0) + w(X_j^k))$; and finally applied the linearity of f and w .

Thus, with some extra effort, we again find $\Delta_0 = 0$ for odd n_0 just as we did for even n_0 . The situation is nevertheless different, since \mathcal{M}_{IJ} now has *four* zero eigenvalues to both zeroth and first order rather than two, meaning that the second-order terms are now proportional to ϵ^8 rather than ϵ^4 .

We thus find that for odd n_0 the leading term of $|\mathcal{M}_{IJ}|$ should be of order l^{2n_0-18} , making the overall distribution of the link length

$$p(l) \sim l^{-2n_0+7+2n_0-18} = l^{-11} \tag{4.46}$$

This, however, makes a long needle far less likely than even a single spike (which we argued above should have at least $p(l) \sim l^{-9}$ in the fermionic case). Thus, it would seem that we should not expect to see needles for odd n_0 .

4.2.3 Higher powers of the determinant

Once we have established the leading behaviour of the determinant, the effect of having higher powers $\gamma > 1$ of \mathcal{M}_{IJ} in the partition function is not difficult to predict. For even n_0 , the determinant should contribute a factor $\sim l^{(2n_0-10)\gamma}$, making the distribution

$$p(l) \sim l^{2n_0(\gamma-1)+7-10\gamma} \tag{4.47}$$

Even for a γ only marginally larger than 1, the result is obviously catastrophic, since the power of the distribution starts to grow linearly with n_0 and will sooner or later reach $p(l) \sim l^{-1}$, at which point the partition function will blow up.

For odd n_0 , the result will be essentially the same, since the exponents simply differ by a constant; for large enough n_0 , the partition function will still become ill-defined.

In other words, we expect an ill-defined partition function if we have no fermions in the model, but also if we include too many fermions; it seems that the only existing model should be the one in which bosonic and fermionic fields are susy-balanced.

4.2.4 Higher dimensions

As promised in the beginning of this chapter, we can easily generalize our arguments for the large l region of the model to the higher-dimensional versions $d = 6$ and $d = 10$.

On a needle with a length scale of order $\sim l$ in d dimensions, we again have one vertex with entirely fixed coordinates, because of the zero mode; one vertex whose d coordinates can all vary freely within a sphere of radius l ; and $n_0 - 2$ vertices with one ‘long’ component in the direction of the needle and $d - 1$ ‘short’ components perpendicular to this direction. The fermionic matrix now has $(d - 2)(n_0 - 1) \times (d - 2)(n_0 - 1)$ entries; by the same arguments as before, the leading term of the determinant will pick up ‘long’ components of order $\sim l$ from all but four rows and ‘short’ components of order $\sim 1/l$ from the remaining ones, so that the contribution from $|\mathcal{M}_{IJ}|^\gamma$ becomes $l^{\gamma(d-2)(n_0-5)}$. Putting it all together and integrating over all but one component gives us the distribution of the link length

$$p(l) = l^{d-1} l^{n_0-2} l^{-(d-1)(n_0-2)} l^{\gamma(d-2)(n_0-5)} = l^{-2d+5+(\gamma-1)(d-2)(n_0-5)} \quad (4.48)$$

For $\gamma > 1$, we again find a partition function that will inevitably blow up if we just take n_0 to be large enough. In the supersymmetric case, however, the n_0 -dependent term once more drops out completely and we find

$$p(l) = l^{-2d+5} \quad (4.49)$$

In particular, we predict $p(l) = l^{-7}$ for $d = 6$ and $p(l) = l^{-15}$ for $d = 10$.

In general, then, we would expect the same qualitative picture in any dimension: the model should have a well-defined partition function in the supersymmetric case, but with a power-law tail of the link length distribution that is dominated by one-dimensional, needle-like configurations, independently of the system size.

4.2.5 Exact solution for the tetrahedron

To further support the power-counting arguments of the preceding sections, we can, as a last point before moving on to the numerical part, solve the model exactly for the smallest possible configuration, *i.e.* the tetrahedron, and show directly that in this case the distribution of the link length is indeed $p(l) \sim l^{-3}$.

First we have to choose a suitable coordinate system. Because of the zero mode, we can fix one of the vertices at the origin, $X_1 = (0, 0, 0, 0)$. Also, we can define the axes, which we will call l , x , y , and z , in such a way that we have one vertex lying on the l axis, one in the (l, x) plane, and one in the (l, x, y) hyperplane: $X_2 = (l_2, 0, 0, 0)$, $X_3 = (l_3, x_3, 0, 0)$, $X_4 = (l_4, x_4, y_4, 0)$.

The bosonic action and fermionic determinant can in these coordinates be calculated as [72, 75]

$$S_B = l_2^2 x_3^2 + (x_3 l_4 - l_3 x_4)^2 + x_4^2 l_2^2 + ((l_2 - l_3) x_4 - (l_2 - l_4) x_3)^2 + 2y_4^2 (l_2^2 + l_3^2 + x_3^2 - l_2 l_3) \quad (4.50)$$

$$|\mathcal{M}_{IJ}| = l_2^2 x_3^2 y_4^2 \quad (4.51)$$

Inserting this into (4.30), we find for the partition function

$$Z(4, 1) = \int_{-\infty}^{\infty} dl_3 dl_4 dx_4 \int_0^{\infty} dl_2 dx_3 dy_4 l_2^5 x_3^4 y_4^3 e^{-S_B} \quad (4.52)$$

The integrations over l_3 , l_4 , x_4 , and y_4 can all be performed, leading to

$$Z(4, 1) = \int_0^{\infty} dl_2 dx_3 \frac{l_2^4 x_3^3}{\sqrt{\frac{3}{4}l_2^2 + x_3^2}} e^{-\frac{4}{3}l_2^2 x_3^2} \quad (4.53)$$

While the last two integrations can also be carried out by an appropriate substitution of variables, thus solving the integral completely, we are more interested in the large l_2 behaviour of the integrand. Because of the exponential part, for a given value of l_2 the second integration variable will make a significant contribution only in the interval $0 \leq x_3 \leq 1/l_2$. If l_2 is large, this interval becomes small, and we can regard the integrand as approximately constant across this range. Thus, we can simply replace $x_3 \rightarrow l_2^{-1}$ and $\int dx_3 \rightarrow l_2^{-1}$, and find that the integral becomes

$$Z(4, 1) \sim Z_{bulk} + \int_L^{\infty} dl_2 l_2^{-3} \quad (4.54)$$

where Z_{bulk} is the contribution of the $l_2 < L$ region to the partition function, and L is large. We can interpret the integrand as a probability distribution for l_2 , valid in the range $l_2 > L$. But l_2 is nothing but the length of the link that connects the vertices $\langle 1 \rangle$ and $\langle 2 \rangle$. Since there is nothing to distinguish this link from any other on the triangulation, we can interpret $p(l) \sim l^{-3}$ as the distribution for *all* link lengths, thus arriving at the same result as before.

4.3 Simulations of the surface model

Our main objective for the numerical simulations will now be to show whether or not our arguments from the preceding sections are correct. Basically, this means we want to prove (or disprove) the following three claims for the model with fermions: spikes are no longer dominant in this case; needles become dominant in the large l region, and actually cause the partition function to diverge when $\gamma > 1$; and needles obey a link length distribution $p(l) \sim l^{-3}$ in the supersymmetric model, or $p(l) \sim l^{2n_0(\gamma-1)+7-10\gamma}$ in general.

4.3.1 Observables

To these ends, we first need to define at least two observables that can function as indicators for the presence of spikes and of needles, respectively. We also have to choose a convenient way of measuring the link length distribution.

Gyration radius and the minimal circle around a vertex

As described in section 4.2.1, the presence of a spike of length l implies that the circle of links around this spike will have a length of order $\sim l^{-1}$. Also, on a configuration dominated by spikes, we can expect the gyration radius (which measures the average extent of the system) to be proportional to the length of the largest spike. Therefore, we would for a spiky triangulation expect an inverse proportion between the gyration radius, which because of the delta function $\delta^4(\sum X_i)$ has the simple form

$$R \equiv \sqrt{\frac{1}{N} \sum X_i^2} \quad (4.55)$$

and the length of the smallest circle of links around a vertex

$$l_c \equiv \min_{\langle i \rangle} \sum_{\langle jk \rangle: \langle ijk \rangle} \sqrt{(X_j - X_k)^2} \quad (4.56)$$

Also, l_c should become arbitrarily small. Conversely, when spikes are absent we would expect no such inverse proportion, and small values of l_c should be suppressed. (In fact, for a needle configuration we would expect a *positive* correlation between l_c and R , since on a needle all link lengths should be of the same order and the gyration radius should be proportional to the average link length.)

Principal component analysis

To decide whether a given configuration is a needle, we have to determine whether it behaves like a one-dimensional structure as a whole. To this end, we first define the correlation matrix

$$C^{\mu\nu} \equiv \frac{1}{N} \sum_{\langle i \rangle} X_i^\mu X_i^\nu \quad (4.57)$$

The eigenvalues r^μ of this matrix can be interpreted as the system's square extent in four independent directions. (Note that the sum of these eigenvalues equals the gyration radius squared, $\sum r^\mu = \text{Tr } C^{\mu\nu} = \frac{1}{N} \sum X_i^2 = R^2$.) The eigenvector belonging to the largest eigenvalue is called the principal axis and designates the direction along which the configuration has its greatest extent.

We can now take each vertex $\langle i \rangle$ on the configuration and calculate its projection on the principal axis, l_i , as well as its distance from it, d_i . From these, we can define the system's overall length and thickness as, respectively,

$$L \equiv \max_{\langle i \rangle \langle j \rangle} (l_i - l_j) \quad (4.58)$$

$$D \equiv \max_{\langle i \rangle} d_i \quad (4.59)$$

The ratio of length to thickness can be used to determine the dimensionality of the system; for sufficiently large values of L/D we would say that the configuration is essentially one-dimensional. In fact, we can put this in more quantitative terms by remembering that, according to our construction, a needle of length L should have a thickness of $\sim L^{-1}$. Since the gyration radius of a one-dimensional configuration is just the same as its length, we can say that for a needle with gyration radius R , we expect a length-to-thickness ratio of order $\sim R^2$. Conversely, for a configuration with spikes, or indeed any four-dimensional system, we should see a ratio of order ≥ 1 .

The distribution of link lengths

While it would certainly be possible to directly measure the distribution of link lengths, we can make our job easier by noting that, as mentioned before, on a needle there should be an approximate proportionality between a typical link length and the gyration radius, $l \sim R$. Since the gyration radius is something we measure anyway, we can simply create a distribution of R and compare it to the power law $p(R) \sim R^{-3}$.

4.3.2 Implementation

For the most part, implementation of the model is straightforward and not too difficult. The greatest problem comes from the rapid increase of *CPU* time required for the calculation of the fermionic determinant, which forces us to keep the system size relatively small.

The part of the algorithm that describes and updates the triangulation itself is based on an earlier program that was written for four-dimensional manifolds [77]. It was re-written in C++ for this project, and becomes much simpler in its two-dimensional version; but the principles remain the same, and I will therefore not describe it here in detail.

The fermionic determinant $|\mathcal{M}_{IJ}|$ is calculated with a standard algorithm based on decomposition of \mathcal{M}_{IJ} into two triangular matrices that was taken from [78]. This algorithm requires of order $o(n_0^3)$ operations for each calculation of the determinant; this is the fastest general method available for this kind of problem.³ Furthermore, we have to perform of order $o(n_0)$ geometrical transformations and field updates to change every part of the triangulation. Finally, we have to repeat this cycle often enough for these local changes to propagate across the entire configuration; some short test runs show that this leads to yet another factor $o(n_0)$. All in all, then, we find that the *CPU* time required to generate a given amount of measurements

³There exists a more specialized method for calculating the determinant of a matrix that differs only in a few elements from a matrix with a known determinant, which could in principle be used here. This method requires only of order $o(n_0^{5/2})$ operations; however, it would have to be performed several times in succession for each updating step, leading to a larger pre-factor for the actual number of operations. Thus, while this method would eventually win over the more general one, it is in fact slower on the small systems that we have to restrict ourselves to.

grows with the system size at least like $\sim n_0^5$. In practice, this limited our studies to surfaces with up to 28 triangles ($n_0 = 16$), plus some preliminary measurements for surfaces with 60 triangles ($n_0 = 32$). The matrix \mathcal{M}_{IJ} itself is stored and updated as required during the simulations, so that it, at least, does not have to be completely re-calculated in each step.

We have to perform two separate kinds of updates: changes in the geometrical structure, and updates of the vertex coordinates. The geometry is altered using the (p, q) moves described in section 2.2.2. As noted there, as long as we are studying a canonical partition function in two dimensions, the only move we actually need is the flip $(2, 2)$.

Apart from the symmetry factors $C(T)$, which are automatically taken care of by the way the (p, q) moves work, there is no weight associated with the geometrical structure that would have to be included in the Metropolis question. However, both the bosonic action and the fermionic matrix are changed by the move. In particular, if we call the original triangles involved in the move $\langle ij k \rangle$ and $\langle j i l \rangle$, we find for the change in the bosonic action

$$\begin{aligned} \Delta S_B = \frac{4}{A} \{ & (X_{kl}^2 - X_{ij}^2) (X_{ij}^2 + X_{ik}^2 + X_{il}^2 + X_{jk}^2 + X_{jl}^2 + X_{kl}^2) \\ & + (X_{il}^2 - X_{jk}^2) (X_{ik}^2 - X_{jl}^2) \} \end{aligned} \quad (4.60)$$

The fermionic matrix has to be updated in twelve different 2×2 ‘blocks’. First of all, since the link $\langle ij \rangle$ is removed by the transformation, all elements associated with it have to be set to zero, $\mathcal{M}_{ij}^{ab} = \mathcal{M}_{ji}^{ab} = 0$. Secondly, the newly created link $\langle kl \rangle$ generates the new elements $\mathcal{M}_{kl}^{ab} = \frac{i}{12} (X_i^\mu - X_j^\mu) \sigma_\mu^{ab}$ and $\mathcal{M}_{lk}^{ab} = \frac{i}{12} (X_j^\mu - X_i^\mu) \sigma_\mu^{ab}$. Finally, the elements associated with the remaining links of the two triangles involved in the move have to be changed by

$$\begin{aligned} \Delta \mathcal{M}_{ik}^{ab} &= \frac{i}{12} (X_j^\mu - X_l^\mu) \sigma_\mu^{ab} & \Delta \mathcal{M}_{ki}^{ab} &= \frac{i}{12} (X_l^\mu - X_j^\mu) \sigma_\mu^{ab} \\ \Delta \mathcal{M}_{il}^{ab} &= \frac{i}{12} (X_k^\mu - X_j^\mu) \sigma_\mu^{ab} & \Delta \mathcal{M}_{li}^{ab} &= \frac{i}{12} (X_j^\mu - X_k^\mu) \sigma_\mu^{ab} \\ \Delta \mathcal{M}_{jk}^{ab} &= \frac{i}{12} (X_l^\mu - X_i^\mu) \sigma_\mu^{ab} & \Delta \mathcal{M}_{kj}^{ab} &= \frac{i}{12} (X_i^\mu - X_l^\mu) \sigma_\mu^{ab} \\ \Delta \mathcal{M}_{jl}^{ab} &= \frac{i}{12} (X_i^\mu - X_k^\mu) \sigma_\mu^{ab} & \Delta \mathcal{M}_{lj}^{ab} &= \frac{i}{12} (X_k^\mu - X_i^\mu) \sigma_\mu^{ab} \end{aligned} \quad (4.61)$$

For a coordinate update, we choose a vertex $\langle i \rangle$ at random and propose a change generated from the interval $[-c, c]$ with a flat distribution, where the parameter c is adjusted so as to produce reasonable acceptance rates (about 60% – 70%). If we leave out the summation indices μ for simplicity and use the notation $\Delta f(X_i) \equiv$

$f(X_i^{new}) - f(X_i^{old})$, we can calculate the change in the bosonic action as

$$\begin{aligned} \Delta S_B = & \frac{4}{A} \left\{ o_i \left((\Delta X_i^2)^2 - \Delta X_i^4 \right) \right. \\ & - 2 \sum_{\langle j \rangle: \langle ij \rangle} \left(X_j^2 \Delta X_i^2 - 2X_j \Delta(X_i^2 X_j) \right. \\ & \quad \left. + 2X_j \Delta X_i^2 \Delta X_i + 2\Delta(X_i X_j)^2 - X_j^2 X_j \Delta X_i \right) \\ & \left. + 2 \sum_{\langle jk \rangle: \langle ijk \rangle} \left(X_{jk}^2 \Delta X_i^2 + 2(\Delta X_i)^2 X_j X_k - (X_j + X_k) X_{jk}^2 \Delta X_i \right) \right\} \end{aligned} \quad (4.62)$$

The fermionic matrix has to be updated in all elements whose lattice indices form a triangle with $\langle i \rangle$, and becomes

$$\Delta \mathcal{M}_{jk}^{ab} = \frac{i}{12} \Delta X_i^\mu \sigma_\mu^{ab} \quad \Delta \mathcal{M}_{kj}^{ab} = -\frac{i}{12} \Delta X_i^\mu \sigma_\mu^{ab} \quad (4.63)$$

where ijk is a clockwise arrangement of the vertices.

As for our chosen observables, the gyration radius R , the smallest circle around a vertex l_c , and the correlation matrix $C_{\mu\nu}$ can all be straightforwardly calculated, since they are all simple functions of the bosonic coordinates X_i^μ . The eigenvalues and eigenvectors of $C_{\mu\nu}$ are determined using a standard algorithm from [78].

A very first test that we can run on the program is a measurement of the average bosonic action, which we can predict from a simple scaling argument. Say we introduce an additional scale factor λ in front of the bosonic action. Symbolically, counting only powers of X , we can then write the partition function as

$$Z(n_2, \gamma, \lambda) = \int (dX)^{4(n_0-1)} X^{2(n_0-1)\gamma} e^{-\lambda X^4} \quad (4.64)$$

If we now make the substitution $X \rightarrow Y \equiv \lambda^{1/4} X$, we find

$$Z(n_2, \gamma, \lambda) = \int \frac{(dY)^{4(n_0-1)}}{\lambda^{n_0-1}} \frac{Y^{2(n_0-1)\gamma}}{\lambda^{\frac{n_0-1}{2}\gamma}} e^{-Y^4} = \lambda^{-\frac{\gamma+2}{2}(n_0-1)} Z(n_2, \gamma, 1) \quad (4.65)$$

From this we can calculate the average bosonic action as

$$\langle S_B \rangle = - \left. \frac{\partial \ln Z}{\partial \lambda} \right|_{\lambda=1} = \frac{\gamma+2}{2} (n_0-1) \quad (4.66)$$

The action can be easily measured in a short numerical run and compared to this formula; we find that they do indeed agree.

Another possible test comes from the analytic calculations for the tetrahedron, from which we actually know for certain that we should find a gyration radius distribution $p(R) \sim R^{-3}$ for large enough R . This also is reproduced by the program, as can be seen in figure 4.1.

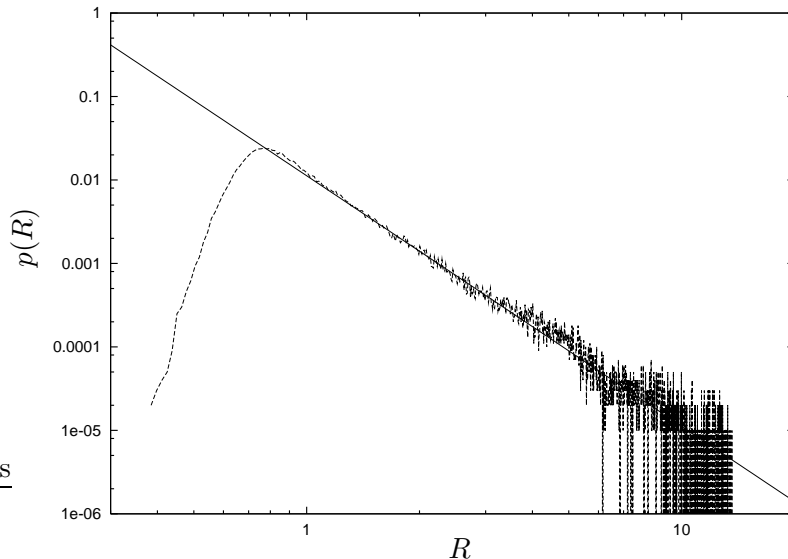


Figure 4.1: The distribution of the gyration radius on the tetrahedron, together with a best fit to a power law $p(R) = aR^{-3}$.

4.3.3 Results

Simulations were performed for values of n_2 up to 28 and $\gamma = 0, 1, 2$. On average, 100000 measurements were performed for each combination (n_2, γ) .

Appearance of spikes

Figure 4.2 shows the gyration radius R versus the length of the shortest circle around a vertex l_c in logarithmic scale, once for the purely bosonic model ($\gamma = 0$) and once for the supersymmetric model ($\gamma = 1$), with the triangulation size $n_2 = 28$ in both cases.

The upper figure shows an obvious inverse proportionality between R and l_c , so we can say that the bosonic model is in fact dominated by spikes. We already knew that, of course, but it does assure us that our method works.

In the supersymmetric case, we see that, as expected, there is no inverse proportionality and, in fact, really small circles are not present at all. Instead, we see the expected positive correlation.

We can therefore conclude that the fermionic determinant does indeed successfully suppress the appearance of spikes.

Appearance of needles

To test for the appearance of needles, we examined configurations that were selected randomly from the region of large gyration radius ($R > 8$), since this is the only

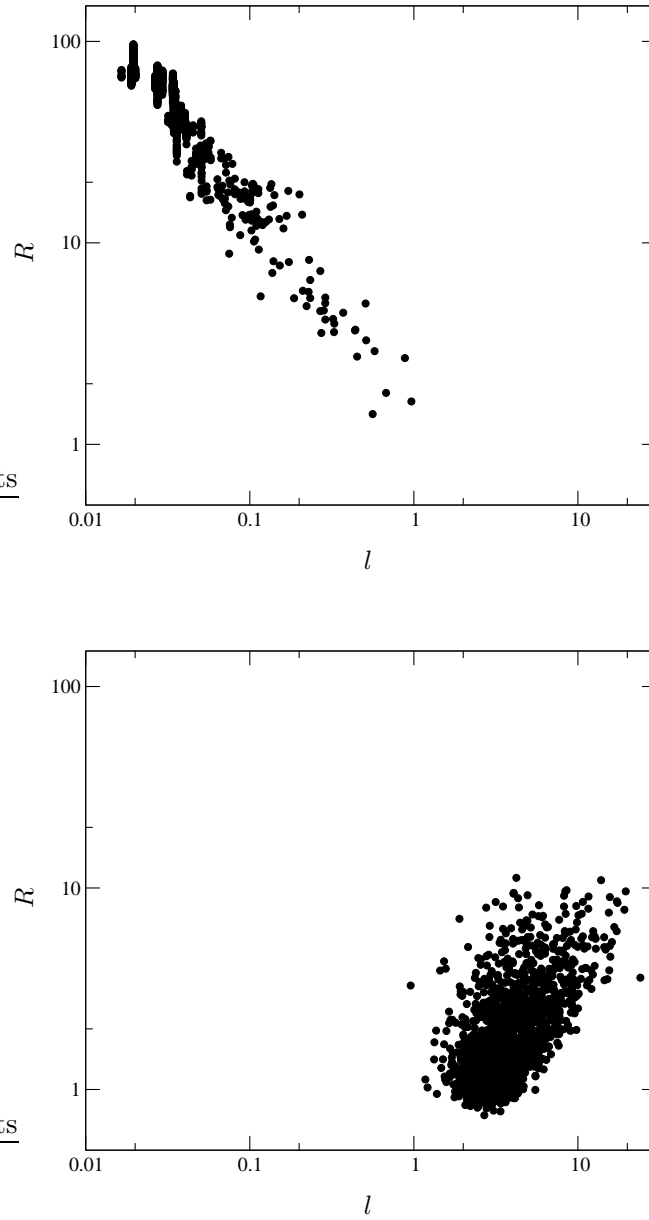


Figure 4.2: The gyration radius R as a function of the shortest loop length l_c , both for the bosonic case (upper figure) and the supersymmetric case (lower figure). The number of triangles is $n_2 = 28$.

regime where we can expect needles.

Figure 4.3 shows snapshots of single configurations after projection onto their respective principal axes. The purely bosonic configuration is clearly not one-dimensional; in fact, we can see directly that this is, not surprisingly, a configuration of spikes. The configuration from the supersymmetric model, on the other hand, shows all vertices lying practically on the principal axis.

Of course, these are only single examples presented here to better illustrate the differences between bosonic and fermionic configurations; by themselves they do not prove anything. But the estimates of the length-to-thickness ratios for the entire runs show us the same thing: we find $L/D = 2.26(8)$ for the bosonic case, and $L/D = 212(20)$ for the fermionic one. These should be compared to our predictions, which were $L/D \sim o(1)$ for the bosonic case and $L/D \sim o(R^2)$ for the fermionic one, with R being restricted to $8 \leq R \leq 10$ for this run. Given that these are only rough estimates of the order of magnitude, the agreement is quite reasonable.

The conclusion, then, is that needles are indeed absent (or more correctly, strongly suppressed) in the bosonic case, while being dominant in the large R region of the fermionic model.

The distribution of R

Finally, we wanted to measure the distribution of the gyration radius. Here we encounter a few technical difficulties due to the power-law tail of the distribution. On the one hand, the tail contains only a few percent of all possible configurations, meaning that if we let the algorithm range freely it will spend most of its time in the bulk of the distribution, drastically increasing the time needed for measurements since we are only really interested in the behaviour of the tail. On the other hand, once the system does enter the tail, it tends to make long excursions to extremely large R every now and then because the power-law behaviour means that there is no natural cut-off. The result is a very large autocorrelation time that, again, means a dramatic increase in the time requirement for each run. The simplest solution to both problems is to set upper and lower limits on R to both prevent uncontrollable excursions and keep the system out of the bulk. The lower limit does have the disadvantage of reducing the acceptance rate of the algorithm because the system constantly tries to go back to the bulk, but we found this to be a much less severe problem than the non-existence of such a limit would be (a factor of about 3 in the acceptance rate as opposed to the system spending about 97% of its time in the bulk if we let it go wherever it wants).

We face a slightly different problem in those cases where the system simply tries to run away to larger and larger R because of a positive power law, as happens when $\gamma > 1$. In these cases, we found it sufficient to simply include an upper limit, since the system does not really try to leave the tail in the direction of lower R anyway. Of course, the system trying to run away is just an indication of the fact that the model is not defined in these cases; we just include them here to show that our predictions for the power laws seem to work universally for any $\gamma \geq 1$.

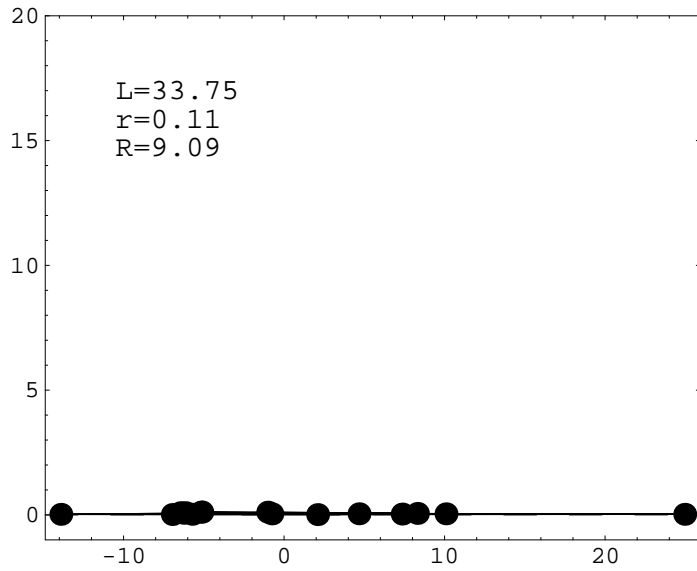
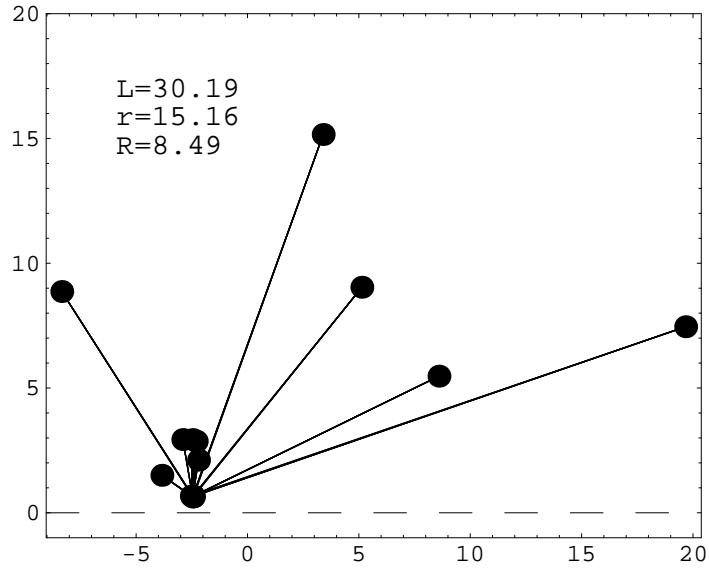


Figure 4.3: Snapshots of large R configurations projected onto their principal axes, both for the bosonic case (upper figure) and the supersymmetric case (lower figure). The x axis shows the position of each point on the principal axis, whereas the y axis shows the point's distance from it. The number of triangles is $n_2 = 28$.

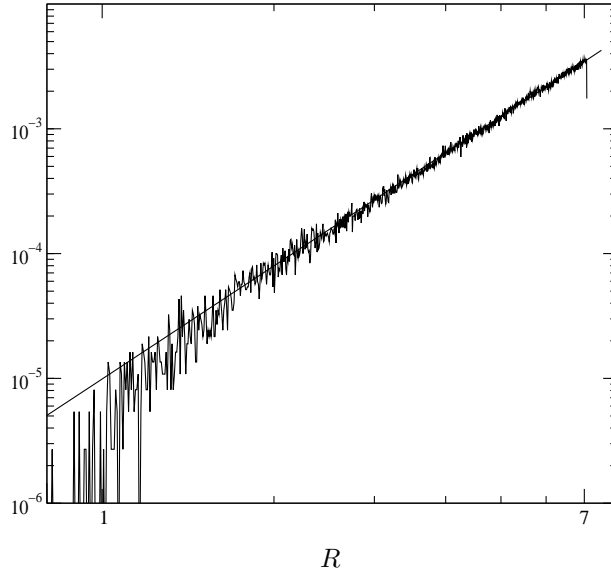
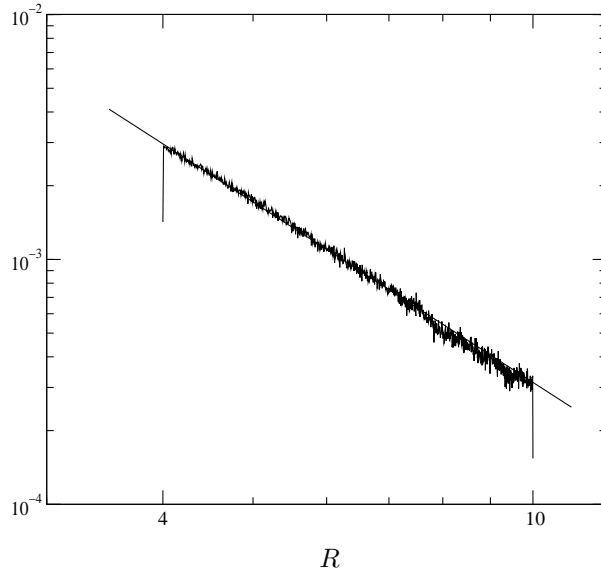


Figure 4.4: The distribution of the gyration radius $p(R)$ for the supersymmetric case (upper figure) and the model with Dirac fermions (lower figure). The numbers of triangles are $n_2 = 28$ and $n_2 = 12$, respectively.

In figure 4.4, I again present two specific results as pictures to show what the distributions look like. The upper figure shows $p(R)$ for $n_2 = 28$ triangles in the supersymmetric case, with lower and upper limits at $R = 4$ and $R = 10$, respectively. The only thing that should be observed is that the distribution does indeed obey a power law. (Note the logarithmic scale.) The same is true for the lower figure, which shows the distribution for the model with Dirac fermions ($\gamma = 2$) and $n_2 = 12$ triangles. The only limit here is an upper boundary at $R = 7$.

Assuming a general power law $p(R) \sim R^\alpha$, we can estimate α for various values of γ and n_2 . The results, together with our theoretical predictions, are presented in the following table:

γ	n_2	α_{num}	α_{the}
1	20	-2.39(4)	-3
1	28	-2.41(3)	-3
1	10	-5.20(1)	-11
1	18	-3.25(1)	-11
2	8	-0.92(2)	-1
2	12	3.02(5)	3
2	16	7.12(12)	7

First of all, we can unequivocally say that in those cases where we expect needles to be dominant to the point of causing actual divergences – *i.e.* for $\gamma > 1$ – the agreement between prediction and simulation is perfect, showing that our mechanism does indeed provide a correct description of what happens in the large R region.

In the supersymmetric case $\gamma = 1$ with $n_2 = 4k$ (corresponding to an even number of vertices), the agreement is obviously less perfect, but we are still in the general vicinity of what we expected. There are several possible explanations for the deviation from the predictions. Most simply, it could just be finite size effects, given that these are really not very large systems. Another possibility is that the results could be influenced by contributions from other configurations, for example because our chosen range of R might still be too near the bulk of the distribution. Finally, there is of course the possibility that our mechanism does work only as a first approximation even for large values of R , but this seems to be contradicted by the positive results for $\gamma = 2$.

As for $\gamma = 1$ and $n_2 = 4k + 2$, the results are obviously totally off, but given the very strong suppression of needles expected from our theoretical arguments in these cases, this apparently just means that there are indeed yet other configurations that are more singular than R^{-11} .

Overall, we would again conclude that the numerical results support our hypothesis, although it should certainly be tried to push simulations of the supersymmetric model to higher values of n_2 so as to get better estimates of the power of the distribution.

4.4 The matrix model

We now turn to an investigation of the *IKKT* model, which was suggested in [61] as a constructive definition of (4.12). This model corresponds to a complete reduction of supersymmetric Yang-Mills theory to 0 dimensions and is therefore also called a Yang-Mills integral. It is defined by

$$Z(n) = \int \mathcal{D}A \mathcal{D}\bar{\Psi} \mathcal{D}\Psi e^{-S(A, \bar{\Psi}, \Psi)} \quad (4.67)$$

where the action is again a sum of a bosonic and a fermionic part,

$$S(A, \bar{\Psi}, \Psi) = S_B(A) + S_F(A, \bar{\Psi}, \Psi) \quad (4.68)$$

$$S_B(A) = -\frac{1}{4} \text{Tr} [A^\mu, A^\nu]^2 \quad (4.69)$$

$$S_F(A, \bar{\Psi}, \Psi) = -\frac{1}{2} \text{Tr} \bar{\Psi}^a \Gamma_\mu^{ab} [A^\mu, \Psi^b] \quad (4.70)$$

Here, A^μ , $\bar{\Psi}^a$, and Ψ^b are $n \times n$ Hermitian matrices, with the entries of $\bar{\Psi}$ and Ψ being Grassmann variables. The model can again be defined as a supersymmetric model in $d = 3, 4, 6$, or 10 dimensions. We will choose $d = 4$ for the same reasons as above.

4.4.1 Needles in the matrix model

Remarkably, the link length distributions (4.49) that we found by applying the needles scenario to the surface model are exactly the same that have been conjectured for the eigenvalue distributions of the matrix model (4.67), based on the only available exact solution that exists for $SU(2)$ [62, 69]. The complete formulas are

$$\begin{aligned} \rho_4(\lambda) &= \frac{6}{\sqrt{2\pi}} \lambda^2 U_\lambda^5 \\ \rho_6(\lambda) &= \frac{105}{2\sqrt{2\pi}} \lambda^2 \left\{ U_\lambda^9 - \frac{33}{16} U_\lambda^{13} \right\} \\ \rho_{10}(\lambda) &= \frac{27027}{64\sqrt{2\pi}} \lambda^2 \left\{ 13U_\lambda^{17} - \frac{2261}{16} U_\lambda^{21} + \frac{334305}{512} U_\lambda^{25} - \frac{5014575}{4096} U_\lambda^{29} \right\} \end{aligned} \quad (4.71)$$

where

$$U_\lambda^a \equiv U \left(\frac{a}{4}, \frac{1}{2}, 4\lambda^4 \right) \quad (4.72)$$

and

$$U(a, b, z) = \frac{1}{\Gamma(a)} \int_0^\infty dt t^{a-1} (1+t)^{b-a-1} e^{-zt} \quad (4.73)$$

is the Kummer U-function. While these formulas look rather unwieldy, their large λ behaviour can be expressed as a simple power law, which is exactly that of the surface model:

$$\rho_d(\lambda) \sim \lambda^{-2d+5} \quad (4.74)$$

While no solution for higher n exists, it was conjectured that this power law should apply independently of n , again just as we found for the surface model.

The obvious question, then, is whether the mechanism that is responsible for this behaviour might also be the same as in the surface model, *i.e.* whether large λ configurations might be one-dimensional needles. Even though the analogies are obvious, it is not *a priori* clear whether we should expect this, since we now lack the geometrical structure of the triangulations, which in our arguments was essential for the formation of needles as a global phenomenon. To take a different example, it is known that spikes do *not* occur in the matrix model – *i.e.* the model is well-defined in the purely bosonic case [68] – exactly because there is no concept of a local geometry or neighbourhood relations between vertices. Nevertheless, a closer look at the behaviour of the matrix model in the large λ region seems definitely worthwhile.

4.4.2 Simulations of the matrix model

Treatment of the model (4.67) to prepare it for numerical simulations is mostly analogous to what we did with the surface model, and I will just briefly sketch the necessary steps.

Since we are still in $d = 4$ dimensions, we can once more use the Weyl condition to replace the four-component spinors $\bar{\Psi}, \Psi$ by two-component ones $\bar{\psi}, \psi$. This makes the fermionic part of the action

$$S_F(A, \psi, \bar{\psi}) = -\frac{1}{2} \text{Tr} \bar{\psi}^a \sigma_\mu^{ab} [A^\mu, \psi^b] \quad (4.75)$$

with $\sigma_0 \equiv i\mathbb{1}$ as before. Expanding the commutator leads to

$$S_F(A, \psi, \bar{\psi}) = -\frac{1}{2} \bar{\psi}_{ij}^a \left(A_{jk}^\mu \sigma_\mu^{ab} \delta_{li} - A_{li}^\mu \sigma_\mu^{ab} \delta_{jk} \right) \psi_{kl}^b \quad (4.76)$$

As with the surface model, we find that the action as it stands has two zero modes coming from a translational symmetry both in the bosonic and in the fermionic sector. We deal with them as before: the bosonic zero mode is fixed by inserting a factor $\delta^4(\sum_i A_{ii}) \equiv \delta^4(\text{Tr}A)$, whereas the fermionic one is removed by skipping the integration over one pair of fermions, which we arbitrarily choose to be $\bar{\psi}_{nn}, \psi_{nn}$.

Integrating over the fermions gives us the determinant of the matrix

$$\mathcal{M}_{ijkl}^{ab} = \frac{1}{2} \left(A_{li}^\mu \sigma_\mu^{ab} \delta_{jk} - A_{jk}^\mu \sigma_\mu^{ab} \delta_{li} \right) \quad (4.77)$$

where $i, j, k, l = 1, \dots, n$ (but excluding the combinations $ij = nn, kl = nn$), and $a, b = 1, 2$. As before, I will usually combine the indices $\binom{a}{ij}, \binom{b}{kl}$ and write the matrix as just \mathcal{M}_{IJ} . The matrix size is now $2(n^2 - 1) \times 2(n^2 - 1)$.

As long as we stay in four dimensions, the determinant $|\mathcal{M}_{IJ}|$ is again real and non-negative. The partition function that we want to simulate is thus

$$Z = \int \prod_{i < j} d^4 \text{Re} A_{ij} d^4 \text{Im} A_{ij} \prod_i d^4 A_{ii} \delta^4(\text{Tr} A) |\mathcal{M}_{IJ}| e^{-S_B(A)} \quad (4.78)$$

Observables

Since, as noted, spikes do not appear in the matrix model, our main objective here is simply the search for needle-like configurations. We can do this in a way similar to what we did before; however, some changes have to be made due to the lack of a geometrical structure in this case.

Namely, this lack of a geometrical interpretation means we will not be able to discern needles by the use of an intuitive quantity like the length-to-thickness ratio L/D that we employed for the surface model. At least, to do so would mean that we would first have to tackle the problem of introducing some sort of commuting coordinates to the model, where for the moment we have only non-commuting matrices. While there exist suggestions for how to do this [66], we would prefer a more direct approach. This can be found in the form of the correlation matrix, which can be defined in analogy to the surface model except that it now also contains quantum fluctuations:

$$C^{\mu\nu} \equiv \frac{1}{N} \text{Tr} A^\mu A^\nu \quad (4.79)$$

On a one-dimensional configuration, we would have all but one of the eigenvalues r_μ of $C^{\mu\nu}$ going towards 0. Our main observable will therefore be the *asymmetry parameter*

$$\eta = \frac{r_2^2 + r_3^2 + r_4^2}{R^2} \quad (4.80)$$

where the eigenvalues have been ordered by size, $r_i \geq r_{i+1}$. If we can show $\eta(R) \rightarrow 0$ for $R \rightarrow \infty$, and show that this holds even with increasing n , we can say that, once again, we see a domination of one-dimensional configurations in the large R regime of the model.

Implementation

In principle, implementation of the matrix model is even easier than it was for the surface theory, since all the geometrical aspects of the triangulations can simply be dropped. The only variables we have to store are the bosonic matrices A_{ij}^μ and the fermionic matrix \mathcal{M}_{IJ} , and there will be no geometrical updates to perform.

The greatest difficulty that we face is again the *CPU* time required to calculate the fermionic determinant. In fact, this problem becomes much worse in the matrix model, since the size of \mathcal{M}_{IJ} now grows with n^2 , meaning that the calculation of the determinant takes of order $o(n^6)$ operations. Also, it will now take of order

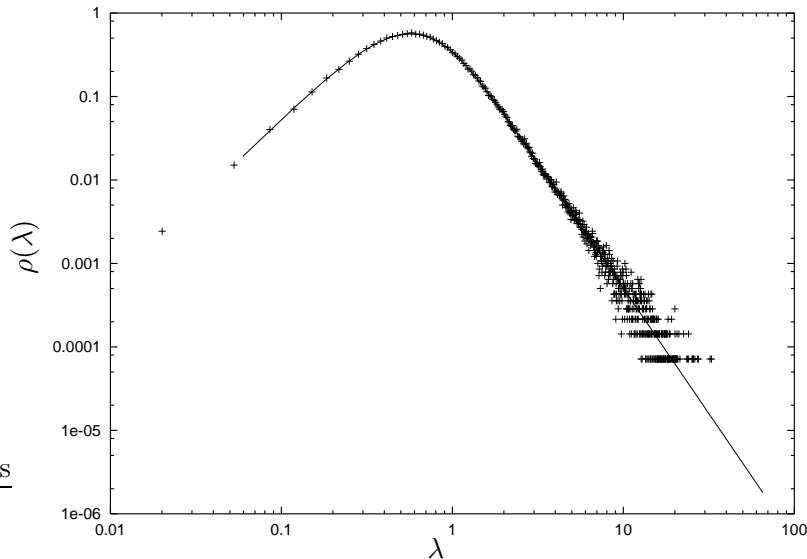


Figure 4.5: The distribution of the eigenvalues of A^μ from the theoretical prediction (solid line) and the numerical data (crosses).

$o(n^2)$ operations to update all the matrix elements, and we find in test runs that the system now requires of order $o(n^2)$ updates for a change to spread across the entire matrix, so that we end up with a *CPU* demand that grows at least with n^{10} . Obviously, we will not be able to go very far with this kind of burden; in practice, we managed to perform measurements up to $SU(8)$ within reasonable timespans.

The program can be tested in ways similar to those we employed in the surface model. The average bosonic action can again be predicted from scaling arguments to be $\langle S_B \rangle = \frac{\gamma+2}{2}(n^2 - 1)$, which is reproduced correctly by the program. Another possibility is measuring the distribution of eigenvalues of A^μ for the case $n = 2$, and comparing it to the theoretical formula (4.72). As figure 4.5 shows, the agreement is perfect.

Results

We will start this section with a look at the case of $SU(2)$, where an analytical treatment of the model is possible. The calculation has been performed in detail elsewhere [62], and I will not repeat it here. Suffice to say that we end up with the following distribution for the eigenvalues of $C^{\mu\nu}$:

$$\rho(r_\mu) \sim \delta(r_4) r_1^\alpha r_2^\alpha r_3^\alpha (r_1^2 - r_2^2)(r_2^2 - r_3^2)(r_3^2 - r_1^2) e^{-2(r_1^2 r_2^2 + r_2^2 r_3^2 + r_3^2 r_1^2)} \quad (4.81)$$

As written, this formula holds in $d = 4$ dimensions, but it remains the same in $d = 6$ and $d = 10$ except for some additional delta functions $\delta(r_5) \dots \delta(r_d)$. The exponent is $\alpha = 2d - 5$ in the fermionic case, or $\alpha = d - 3$ in the bosonic one.

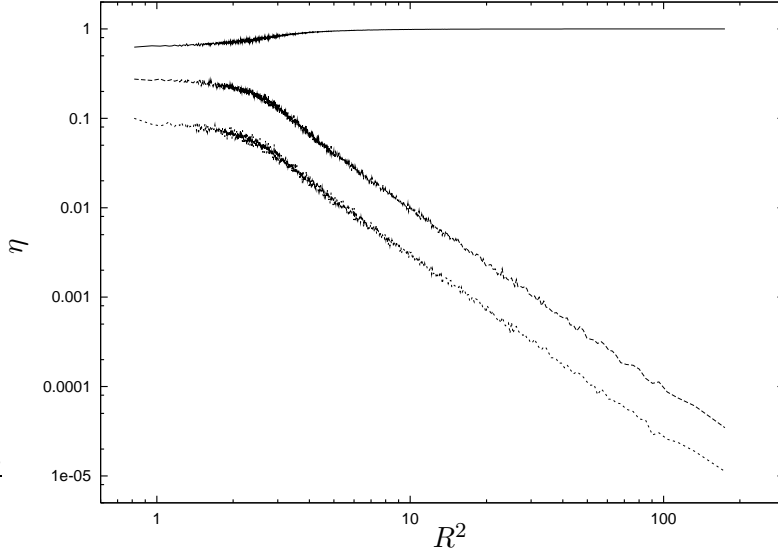


Figure 4.6: The eigenvalues $r_{1,2,3}^2/R^2$ as functions of R^2 for $n = 2$. Note that the data has been smoothed so that each point actually represents an average $(\overline{R^2}, \overline{r^2/R^2})$, taken over 100 successive values of R^2 .

From this formula we can now extract the behaviour of the model for large values of $R^2 = r_1^2 + r_2^2 + r_3^2$. These large values will be exponentially suppressed unless we can arrange the eigenvalues in just such a way that the term $r_1^2 r_2^2 + r_2^2 r_3^2 + r_3^2 r_1^2$ remains of order 1. Since at least one eigenvalue must become large in order for R^2 to grow, this is only possible if $r_1^2 \sim R^2$, $r_{2,3}^2 \leq R^{-2}$. As before, we can approximately describe this behaviour by replacing $r_1 \rightarrow R$, $r_{2,3} \rightarrow R^{-1}$, and $\int dr_{2,3} \rightarrow R^{-1}$, which makes the distribution for R

$$p(R) \sim R^{-\alpha} \quad (4.82)$$

as expected. Again, then, we find a power-law tail of the distribution as a consequence of a flat direction in the exponential part of the action. Also, from the arguments above we can expect the asymmetry parameter to behave as

$$\eta = \frac{r_2^2 + r_3^2}{R^2} \sim \frac{1}{(R^2)^2} \rightarrow 0 \quad (4.83)$$

so we should once more see a dominance of one-dimensional configurations in the large R region.

This is exactly what we find in numerical simulations of the $SU(2)$ case. The results of the measurements are presented in figure 4.6; we see that only the largest eigenvalue does not go to zero with increasing R^2 . For the others we find a power law $r_i^2/R^2 \sim a_i (R^2)^{b_i}$; a best fit of the exponents yields $b_2 = -2.04(2)$ and $b_3 = -2.02(3)$, to be compared to the prediction $b_{2,3} = -2$.

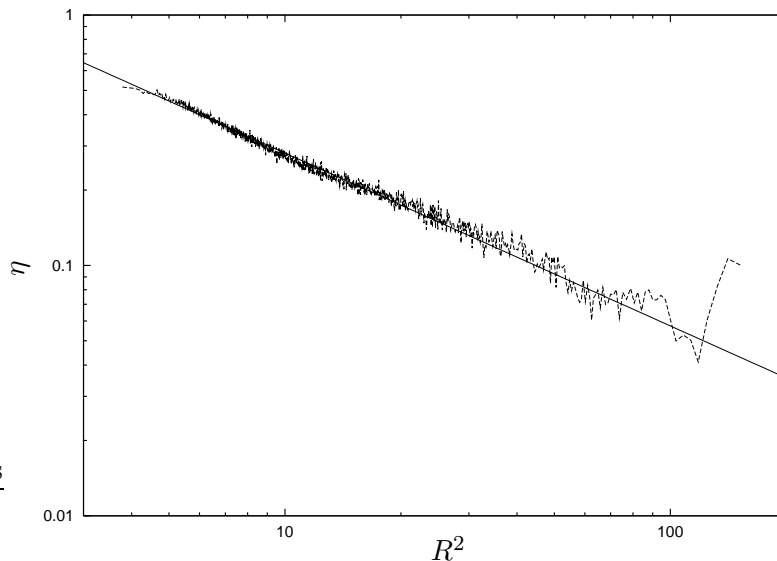


Figure 4.7: The asymmetry parameter $\eta = \frac{r_2^2 + r_3^2 + r_3^2}{R^2}$ as a function of R^2 , for $n = 4$. The data has been smoothed as explained for figure 4.6. The solid line represents the best fit to a power law.

For $n > 2$, no analytic solutions exist, and we have to contend ourselves with numerical measurements of η and its distribution. One typical plot, for $n = 4$, is shown in figure 4.7; it is obvious that we again have a power law $\eta = a(R^2)^b$. A best fit of the parameters to the data yields $a = 1.378(7)$ and $b = -0.690(4)$. As a test to see whether this power law remains stable when we go with R^2 to infinity, we repeated the run with a lower bound imposed on the gyration radius, $R_{min}^2 = 120$, and found that the resulting curve was well described by the same power law.

Overall, we performed simulations for matrix sizes up to $n = 8$. Repeating the calculations from above leads to the following exponents for the power law:

n	b
3	-0.825(2)
4	-0.690(4)
5	-0.606(4)
6	-0.562(5)
8	-0.503(29)

While we do see a negative power in all cases, its absolute value clearly becomes smaller with n , so it is vital to know whether it always stays negative or goes towards 0 in the large n limit. We can try to make a prediction by assuming various types of finite size corrections $b(n) = b_\infty + c/n^p$ to the limiting value; taking the power of n to be $p = 1, 1.5,$ and 2 , we find $b_\infty = -0.30(3), -0.41(2),$ and $-0.47(2)$, respectively.

Alternatively, if we include p as a free variable in the fit, we find $b_\infty = -0.37(11)$ and $p = 1.26(40)$.

With some due caution because of our limited data, we would from these values conclude that b does indeed remain negative in the large n limit. Thus we can say that we again see one-dimensional configurations in the large R regime, and that this phenomenon seems to be preserved even when going to larger n .

4.5 Discussion

When we look at the results found for the surface and matrix models from both theoretical conjectures and numerical simulations, we see a consistent picture emerging for both models. The crucial point lies in the fact that we have an area action – a sum over triangle areas in the discretized surface model; a commutator of matrices as the corresponding quantity in the matrix model. This action successfully suppresses configurations with a large two- or higher-dimensional extent, but is insensitive to a deformation of surfaces (or matrix eigenvalues) to an elongated state in only one dimension, provided that the other directions are simultaneously contracted in a way that leaves the area unchanged. The result is a distribution of link lengths (or eigenvalues) with a power-law tail $p(l) \sim l^{-2d+5}$ for any finite system size, a prediction that, while admittedly a conjecture without rigorous proof, has been arrived at independently in both models and approximately reproduced in numerical simulations. In the case of bosonic surface models, the impact of these needle-like configurations is blotted out by the appearance of an even more singular phenomenon, namely multiple spikes; otherwise, the mechanism seems to be essentially the same in both models.

An interesting point is that we can change the dimensionality of the elongated structures by a simple adaptation of the action. For example, if we replace the ‘area action’ of the matrix model $S_B \sim \text{Tr}[A^\mu, A^\nu]^2$ by another term

$$S_B \sim \text{Tr}[A^\mu, A^\nu][A^\nu, A^\rho][A^\rho, A^\mu] \quad (4.84)$$

we find a new model with the same symmetries as the old one, but also with the possibility of two-dimensional elongated structures. Namely, the distribution of eigenvalues of the correlation matrix now becomes, at least in the case of $SU(2)$ which we can solve,

$$\rho(r_i) \sim \delta(r_4) \dots \delta(r_d) r_1^\alpha r_2^\alpha r_3^\alpha (r_1^2 - r_2^2) (r_2^2 - r_3^2) (r_3^2 - r_1^2) e^{-24r_1^2 r_2^2 r_3^2} \quad (4.85)$$

If we again look for possibilities of going to large values of R^2 while keeping the exponential part of the distribution constant, we see that now a choice of $r_{1,2} \sim R$, $r_3 \sim R^{-2}$ will do the trick – a choice that obviously describes a two-dimensional surface rather than a one-dimensional needle. Taking this argument even further, we could probably create k -dimensional surfaces in the large R region for any $k < d$. In particular, we might build a ten-dimensional model that at large distances contracts

to four dimensions. While this is an intriguing possibility, for the moment we do not yet know how to motivate such a change of the action.

An as yet unsolved question concerning our discoveries is the behaviour of the model if we were to actually take the system size (n_2 or n , respectively) to infinity. We can state with fair confidence that the exponent in the power law is independent of n , but that still leaves the possibility of a prefactor that might vanish with $n \rightarrow \infty$. In fact, if we were to assume all link lengths as independent, then the central limit theorem of statistics would tell us that the distribution of R , which can be written as a sum of all link lengths, should become Gaussian in the large n limit. On the other hand, it is not at all clear whether we should take independence of the link lengths as a given; actually, one basic assumption in our power counting arguments was that all link lengths should be of the same order, which directly contradicts independence. Also, the model that presumably forms the large n limit of both models has itself an area action, so it actually seems quite plausible that it should allow the same kind of one-dimensional structures. Nevertheless, for a definite answer this point clearly has to be examined further, which at the time of writing of this thesis was still a work in progress.

Chapter 5

Summary

In this thesis I have examined two different models of random geometries and their discretizations in terms of dynamical triangulations. Both models have been studied in simpler forms before, but turned out to have difficulties; here, we applied modifications designed to stabilize their behaviour. In both cases, we observed considerable changes as a result of these modifications.

In four-dimensional simplicial quantum gravity, we followed a suggestion, based on a study of the effective action for the conformal factor, that the model might need a minimum amount of matter for a continuum limit to exist. We studied the model with a variable amount of vector fields, and indeed found that starting with $n_V = 3$ the phase structure becomes significantly altered. Namely, the strong coupling phase, which in the pure gravity model is dominated by essentially one-dimensional branched polymers, is replaced by a four-dimensional universe with a negative string susceptibility exponent. We were also able to show that the same effect can be achieved by the inclusion of an additional measure term $\prod o_i^\beta$ if β is taken to be large enough and negative. This is the first time that such a fundamental deviation from the pure gravity behaviour has been observed.

The new so-called crinkled phase that is created in this way still faces some uncertainties that we were unable to resolve on the comparatively small surfaces examined here; in particular, the pseudo-critical value of the coupling constant $\kappa_2^c(n_4)$ grows with the system size in a way that makes it difficult to decide whether it will converge to a finite value in the large n_4 limit. This question can only be addressed in further studies of much larger systems. Alternatively, an examination of a model that includes both vector and fermion fields also seems promising.

This project also allowed us to test the applicability of the strong coupling expansion as a non-statistical method to four-dimensional simplicial quantum gravity. We were able to show that for large enough values of the coupling constant, the predictions for the susceptibility exponent from the strong coupling expansion are well compatible with the numerical results. This allowed us to perform much more thorough studies of the effects of varying parameters such as n_V or β , since the series terms have to be calculated only once, after which the re-calculation of observables

for different parameter values takes almost no extra time. A very practical problem we still face, however, is to find more general methods for extracting observables from the expansion while reducing the finite size effects.

The other project we explored was the discretization of quantum string theory based on a re-formulation of the *IIB* superstring, in the hope that the addition of fermions might cure the diseases observed in the model of bosonic strings. This did in fact turn out to be true; our numerical studies show that the geometrical defects known as spikes are much more strongly suppressed in the supersymmetric case, and in particular are no longer able to create divergences in the partition function of the model. Instead, we see a different kind of geometrical deformation emerging that in the case of ‘too many’ fermions again leads to divergent contributions to the partition function. In the supersymmetric case, however, we can show that the model does indeed become well-defined.

Differently from spikes, the ‘new’ kind of geometrical deformation that is enhanced by the fermions turns out to be a global phenomenon of thin, needle-like surfaces. Being essentially one-dimensional, these structures are ‘invisible’ to the model’s area-type action, which means that they are not exponentially suppressed as one would usually suspect. Instead, from power-counting arguments we were able to predict that they should be governed by a power law with an exponent that is independent from the system size; this we were also able to confirm numerically. While our numerical simulations extend only to the four-dimensional version of the model, our theoretical arguments predict the same kind of behaviour in any dimension, with the only difference being a change in the exponent of the power law.

A curious parallel between this model and the d -dimensional generalization of the *IKKT* matrix model, where exactly the same power laws were observed for the distribution of the matrix eigenvalues, led us to repeat our simulations in the context of this model. Indeed, we were again able to show the emergence of one-dimensional structures in the region of large eigenvalues. This is not very surprising, since the model has a sort of matrix analogue to the area-type action that was responsible for these structures in the surface model. A question that still has to be investigated further is whether or not these things can be expected to survive in the large n limit, although it seems plausible that they should.

Acknowledgments

First and foremost, I would like to thank Prof. B. Petersson for, well, everything really; without his constant support and advice, helpful ideas, and the occasional friendly prodding for results when I needed it, this thesis never would have been written at all. Many thanks must also go to Z. Burda, for being infinitely patient in the face of a thousand silly and repeated questions. Finally, I would like to thank all the people that I worked with over the last four years, in particular P. Bialas, S. Bilke, G. Thorleifsson, and M. Wattenberg. It has been fun.

Bibliography

- [1] D. Weingarten, Phys. Lett. B90 (1980) 280.
- [2] B. Baumann and B. Berg, Phys. Lett. B164 (1985) 131.
- [3] S. Bilke, *Studies in random geometries: Hypercubic random surfaces and simplicial quantum gravity* (doctoral thesis), [hep-lat/9805006](#)
- [4] F. David, *Simplicial quantum gravity and random lattices*, Proc. Les Houches Summer School 92 (1992) 679.
- [5] T. Regge, Nuovo Cim. 19 (1961) 558.
- [6] M. Rocek and R. Williams, Phys. Lett. B104 (1981) 31.
- [7] J. Ambjørn, Nucl. Phys. (Proc. Suppl.) B42 (1995) 3.
- [8] C. Holm and W. Janke, Phys. Lett. B375 (1996) 69.
- [9] F. David, Nucl. Phys. B257 (1985) 45.
- [10] J. Ambjørn, B. Durhuus and J. Fröhlich, Nucl. Phys. B257 (1985) 433.
- [11] V. Kazakov, I. Kostov and A. Migdal, Phys. Lett. B157 (1985) 295.
- [12] J. Ambjørn, Z. Burda, J. Jurkiewicz and C. Kristjansen, Acta Phys. Polon. B23 (1992) 991.
- [13] B. Brüggmann and E. Marinari, Phys. Lett. B349 (1995) 35.
- [14] S. Bilke, Z. Burda and B. Petersson, Phys. Lett. B395 (1997) 4.
- [15] S. Bilke, Z. Burda, A. Krzywicki and B. Petersson, Nucl. Phys. (Proc. Suppl.) 53 (1997) 743.
- [16] M. Gross and S. Varsted, Nucl. Phys. B378 (1992) 367.
- [17] J. Alexander, Ann. Math. 31 (1930) 292.
- [18] D. Boulatov, V. Kazakov, I. Kostov and A. Migdal, Nucl. Phys. B275 (1986) 641.

- [19] G. Thorleifsson, Nucl. Phys. B538 (1999) 278.
- [20] S. Bilke and G. Thorleifsson, Phys. Rev. D59 (1999) 124008.
- [21] S. Hawking and W. Israel, *An Einstein centenary survey*, Cambridge University Press 1979.
- [22] S. Hawking, Commun. Math. Phys. 43 (1975) 199.
- [23] G. Gibbons and M. Perry, Proc. Roy. Soc. Lond. A358 (1978) 467.
- [24] D. Boulatov and A. Krzywicki, Mod. Phys. Lett. A6 (1991) 3005.
- [25] J. Ambjørn, D. Boulatov and A. Krzywicki, Phys. Lett. B276 (1992) 432.
- [26] M. Agishtein and A. Migdal, Nucl. Phys. B385 (1992) 395.
- [27] J. Ambjørn and J. Jurkiewicz, Phys. Lett. B278 (1992) 42.
- [28] J. Ambjørn, B. Durhuus, J. Fröhlich and P. Orland, Nucl. Phys. B270 (1986) 457.
- [29] J. Ambjørn, B. Durhuus and J. Fröhlich, Nucl. Phys. B275 (1986) 161.
- [30] J. Ambjørn, Trieste Spring School 1993 (1993) 228.
- [31] V. Knizhnik, A. Polyakov and A. Zamolodchikov, Mod. Phys. Lett. A3 (1988) 819.
- [32] F. David, Mod. Phys. Lett. A3 (1988) 1651.
- [33] J. Distler and H. Kawai, Nucl. Phys. B321 (1989) 509.
- [34] M. Cates, Europhys. Lett. 8 (1988) 719.
- [35] A. Krzywicki, Phys. Rev. D41 (1990) 3086.
- [36] F. David, Nucl. Phys. B368 (1992) 671.
- [37] P. Bialas, Z. Burda, B. Petersson and J. Tabaczek, Nucl. Phys. B495 (1997) 463.
- [38] P. Bialas, Z. Burda, A. Krzywicki and B. Petersson, Nucl. Phys. B472 (1996) 293.
- [39] B. de Bakker, Phys. Lett. B389 (1996) 238.
- [40] J. Ambjørn, J. Jurkiewicz and C. Kristjansen, Nucl. Phys. B393 (1993) 601.
- [41] I. Antoniadis and E. Mottola, Phys. Rev. D45 (1992) 2013.
- [42] I. Antoniadis, P. Mazur and E. Mottola, Nucl. Phys. B388 (1992) 627.

- [43] I. Antoniadis, P. Mazur and E. Mottola, Phys. Lett. B394 (1997) 49.
- [44] J. Ambjørn, Z. Burda, J. Jurkiewicz and C. Kristjansen, Phys. Rev. D48 (1993) 3695.
- [45] N. Christ, R. Friedberg and T. Lee, Nucl. Phys. B210 (1982) 310.
- [46] N. Christ, R. Friedberg and T. Lee, Nucl. Phys. B210 (1982) 337.
- [47] S. Bilke, Z. Burda, A. Krzywicki, B. Petersson, J. Tabaczek and G. Thorleifsson, Phys. Lett. B418 (1998) 266.
- [48] S. Bilke, Z. Burda, A. Krzywicki, B. Petersson, J. Tabaczek and G. Thorleifsson, Phys. Lett. B432 (1998) 279.
- [49] F. David, Nucl. Phys. B257 (1985) 543.
- [50] F. David, J. Jurkiewicz, A. Krzywicki and B. Petersson, Nucl. Phys. B290 (1987) 218.
- [51] P. Bialas, B. Petersson and G. Thorleifsson, Nucl. Phys. B550 (1999) 465.
- [52] J. Ambjørn, M. Carfora and A. Marzuoli, *The geometry of dynamical triangulations*, hep-th/9612069
- [53] P. Bialas, Z. Burda and D. Johnston, Nucl. Phys. B493 (1997) 505.
- [54] P. Bialas and Z. Burda, Phys. Lett. B416 (1998) 281.
- [55] P. Bialas, Z. Burda and D. Johnston, Nucl. Phys. B542 (1999) 413.
- [56] H. Egawa, S. Horata, N. Tsuda and T. Yukawa, Nucl. Phys. (Proc. Suppl.) 83 (2000) 751.
- [57] J. Ambjørn, K. Anagnostopoulos and J. Jurkiewicz, JHEP 9908 (1999) 16.
- [58] A. Polyakov, Phys. Lett. B103 (1981) 207.
- [59] A. Polyakov, Phys. Lett. B103 (1981) 211.
- [60] M. Green, J. Schwarz and E. Witten, *Superstring theory*, Cambridge University Press 1987.
- [61] N. Ishibashi, H. Kawai, Y. Kitazawa and A. Tsuchiya, Nucl. Phys. B498 (1997) 467.
- [62] H. Aoki, S. Iso, H. Kawai, Y. Kitazawa and A. Tada, Prog. Theor. Phys. 99 (1998) 713.
- [63] H. Aoki, S. Iso, H. Kawai, Y. Kitazawa, A. Tada and A. Tsuchiya, Prog. Theor. Phys. Suppl. 134 (1999) 47.

- [64] J. Nishimura and G. Vernizzi, JHEP 0004 (2000) 15.
- [65] J. Ambjørn, K. N. Anagnostopoulos, W. Bietenholz, T. Hotta and J. Nishimura, JHEP 0007 (2000) 11.
- [66] J. Ambjørn, K. N. Anagnostopoulos, W. Bietenholz, T. Hotta and J. Nishimura, JHEP 0007 (2000) 13.
- [67] W. Krauth, H. Nicolai and M. Staudacher, Phys. Lett. B431 (1998) 31.
- [68] W. Krauth and M. Staudacher, Phys. Lett. B453 (1999) 253.
- [69] W. Krauth, J. Plefka and M. Staudacher, Class. Quant. Grav. 17 (2000) 1171.
- [70] A. Mikovic and W. Siegel, Phys. Lett. B240 (1990) 363.
- [71] J. Ambjørn and S. Varsted, Phys. Lett. B257 (1991) 305.
- [72] S. Oda and T. Yukawa, Prog. Theor. Phys. 102 (1999) 215.
- [73] M. Green and J. Schwarz, Phys. Lett. B136 (1984) 367.
- [74] A. Schild, Phys. Rev. D16 (1977) 1722.
- [75] P. Bialas, Z. Burda, B. Petersson and J. Tabaczek, Nucl. Phys. B592 (2001) 391.
- [76] Z. Burda, B. Petersson and J. Tabaczek, *Geometry of reduced supersymmetric 4d Yang-Mills integrals*, hep-lat/0012001, to be published in Nucl. Phys.
- [77] S. Bilke, Z. Burda and J. Jurkiewicz, Comput. Phys. Commun. 85 (1995) 278.
- [78] W. Press, *Numerical Recipes*, Cambridge University Press 1997.